



Published in final edited form as:

Nature. 2020 January ; 577(7792): 676–681. doi:10.1038/s41586-020-1935-3.

Hyperactivation of Sympathetic Nerves Drives Melanocyte Stem Cell Depletion

Bing Zhang¹, Sai Ma^{1,2,9}, Inbal Rachmin³, Megan He^{1,4}, Pankaj Baral⁵, Sekyu Choi¹, William A. Gonçalves⁶, Yulia Schwartz¹, Eva M. Fast^{1,7}, Yiqun Su³, Leonard I. Zon^{1,7,8}, Aviv Regev^{2,8,9}, Jason D. Buenrostro¹, Thiago M. Cunha^{5,10}, Isaac M. Chiu⁵, David E. Fisher³, Ya-Chieh Hsu^{1,*}

¹Department of Stem Cell and Regenerative Biology, Harvard University and Harvard Stem Cell Institute, Cambridge, MA, USA

²Klarman Cell Observatory, Broad Institute of MIT and Harvard, Cambridge, MA, USA

³Cutaneous Biology Research Center, Department of Dermatology, Massachusetts General Hospital, Harvard Medical School, Charlestown, MA, USA

⁴Molecules, Cells, and Organisms PhD Program, Department of Molecular and Cellular Biology, Harvard University, Cambridge, MA, USA

⁵Department of Immunology, Harvard Medical School, Boston, MA, USA

⁶Graduate Program in Cellular Biology, Institute of Biological Science, Federal University of Minas Gerais, Belo Horizonte, MG, Brazil

⁷Stem Cell Program and Division of Hematology/Oncology, Boston Children's Hospital and Dana-Farber Cancer Institute, Harvard Medical School, Boston, MA, USA

Reprints and permissions information is available at <http://www.nature.com/reprints>. Users may view, print, copy, and download text and data-mine the content in such documents, for the purposes of academic research, subject always to the full Conditions of use: http://www.nature.com/authors/editorial_policies/license.html#terms

*Correspondence to: Ya-Chieh Hsu, PhD (**Lead Contact**), yachieh_hsu@harvard.edu.

AUTHOR CONTRIBUTIONS

B.Z. and Y-C.H. conceived the project. B.Z. performed most of the experiments. S.M. performed bioinformatic analysis. I.R. and Y.Su performed the human melanocyte experiments. M.H. performed the sympathetic ganglia immunostaining and sympathetic nerve density quantifications. P.B. and I.M.C. made the initial observations of hair greying in RTX-injected mice. S.C. performed experiments related to CUS and corticosterone feeding. Y. Schwartz performed the sympathetic nerve ablation experiments. W.A.G. and T.M.C. performed the guanethidine experiments. E.M.F. performed the radiation experiments. Y-C.H., D.E.F., I.M.C., T.M.C., J.D.B., A.R. and L.I.Z. provided intellectual inputs and helped shape the research. B.Z. and Y-C.H. wrote the manuscript with discussions and feedback from all co-authors.

COMPETING INTERESTS

L.I.Z. is a founder and stockholder of Fate Therapeutics, Inc., Scholar Rock and Camp4 Therapeutics. D.E.F. has a financial interest in Soltego, Inc., a company developing SIK inhibitors for topical skin darkening treatments that might be used for a broad set of human applications. D.E.F.'s interests were reviewed and are managed by Massachusetts General Hospital and Partners HealthCare in accordance with their conflict of interest policies. A.R. is an SAB member of ThermoFisher Scientific, Neogene Therapeutics, Asimov, and Syros Pharmaceuticals, an equity holder of Immunitas, and a founder and an equity holder of Celsius Therapeutics. I.M.C. is an SAB member of GSK pharmaceuticals and Kintai pharmaceuticals. A provisional patent application has been filed based on this work (Applicants: President and Fellows of Harvard College and The General Hospital Corporation; Inventors: Y-C.H., D.E.F., B.Z., and I.R.; Application number: 62/903,517; Status: pending/provisional; Aspect covered: Methods and compositions for controlling hair greying. All other authors declare no competing interests.

DATA AVAILABILITY

Sequence data that support the findings of this study have been deposited in GEO with the accession codes GSE131566 (<https://www.ncbi.nlm.nih.gov/geo/query/acc.cgi?acc=GSE131566>).

Source data for all figures are provided with the paper.

⁸Howard Hughes Medical Institute, Chevy Chase, MD, USA

⁹Department of Biology and Koch Institute, Massachusetts Institute of Technology, Cambridge, MA, USA

¹⁰Center for Research in Inflammatory Diseases (CRID), Department of Pharmacology, Ribeirão Preto Medical School, University of São Paulo, Av. Bandeirantes, 3900, Ribeirão Preto, SP, Brazil

SUMMARY

Empirical and anecdotal evidence have associated stress with accelerated hair greying (formation of unpigmented hairs)^{1,2}, but the scientific evidence linking the two is scant. Here, we report that acute stress leads to hair greying through fast depletion of melanocyte stem cells (MeSCs). Combining adrenalectomy, denervation, chemogenetics^{3,4}, cell ablation, and MeSC-specific adrenergic receptor knockout, we found that stress-induced MeSC loss is independent of immune attack or adrenal stress hormones. Rather, hair greying results from activation of the sympathetic nerves that innervate the MeSC niche. Upon stress, sympathetic nerve activation leads to burst release of the neurotransmitter norepinephrine, which drives quiescent MeSCs into rapid proliferation, followed by differentiation, migration, and permanent depletion from the niche. Transient suppression of MeSC proliferation prevents stress-induced hair greying. Our studies demonstrate that acute stress-induced neuronal activity can drive rapid and permanent loss of somatic stem cells, and illustrate an example in which somatic stem cell maintenance is directly influenced by the overall physiological state of the organism.

Stress has been anecdotally associated with diverse tissue changes including hair greying. However, whether external stressors indeed are the causal factors, and if stress-related changes occur at the level of somatic stem cells, remain poorly understood. The hair follicle cycles between growth (anagen), degeneration (catagen), and rest (telogen)⁵. The bulge and hair germ region harbours two stem cell populations—epithelial-derived hair follicle stem cells (HFSCs) and neural crest-derived MeSCs⁶. HFSCs and MeSCs are normally quiescent except during early anagen, when HFSCs and MeSCs are activated concurrently to regenerate a pigmented hair^{7,8}. Activation of HFSCs produces a new hair follicle. Activation of MeSCs generates differentiated melanocytes that migrate downward, while MeSCs remain close to the bulge. At the hair bulb, differentiated melanocytes synthesize melanin to colour the newly regenerated hair from the root. At catagen, mature melanocytes are destroyed, leaving only the MeSCs that will initiate new rounds of melanogenesis in future cycles (Extended Data Fig. 1a)^{9,10}. The stereotypic behaviour of MeSCs and melanocytes, as well as the visible nature of hair colour, makes the melanocyte lineage an accessible model to investigate how stress influences tissue regeneration.

Diverse stressors induce hair greying

To examine whether psychological or physical stressors promote hair greying, we used three approaches to model stress in black coat colour C57BL/6J mice: restraint stress^{11,12}, chronic unpredictable stress^{13,14}, and nociception-induced stress via injection of resiniferatoxin (RTX, a capsaicin analogue)^{15,16}. All three procedures led to increased numbers of unpigmented white hairs over time. Restraint stress and chronic unpredictable stress led to

noticeable hair greying after 3–5 rounds of hair cycles. Nociception-induced stress produced the most pronounced and rapid effect—many new hairs formed in the next hair cycle following RTX injection became unpigmented (Fig. 1a, b, Extended Data Fig. 1b, c).

Psychological or physical stressors trigger the adrenal glands to release stress hormones and catecholamines into the bloodstream¹⁷. Indeed, we detected an increase in both corticosterone (cortisol equivalent in rodents; a stress hormone) and norepinephrine (a catecholamine) in the blood of mice subjected to different stressors (Fig. 1c, Extended Data Fig. 1d), suggesting that our approaches induced classical stress responses.

RTX induces nociception by activating nociceptive sensory neurons¹⁸. Blocking the ability of an animal to sense pain with buprenorphine (an opioid analgesia) prevents the increase of corticosterone and norepinephrine after RTX injection, suggesting that blocking pain sensation alleviates the physiological stress responses induced by RTX (Fig. 1c). Moreover, buprenorphine also suppressed white hair formation in RTX-injected animals (Fig. 1d). These data show that regardless of stress modality, premature hair greying can occur under stress. Because the effect of nociception induction on hair greying was the strongest and most rapid of all stressors tested, we focused on RTX injection as our primary stressor.

Stress leads to loss of MeSCs

Loss of hair pigmentation can be due to defects in melanin synthesis^{19,20}, loss of differentiated melanocytes²¹, or problems in MeSC maintenance²². To understand how stress impacts the melanocyte lineage, we injected RTX into mice in anagen, when both MeSCs and differentiated melanocytes were present but located within distinct compartments—MeSCs were near to the bulge while differentiated melanocytes were at the hair bulb (Fig. 1e). Upon RTX injection, TRP2+ MeSCs were significantly reduced across the entire skin (Fig. 1e, bar graph). In many hair follicles, MeSCs were lost completely from the bulge within 5 days, while differentiated melanocytes in the same hair follicle remained unperturbed (Fig. 1e, D5 after RTX, Extended Data Fig. 1e). These differentiated melanocytes continued to generate pigments, and the hair coat remained black (Extended Data Fig. 1f, g). When hair follicles in the RTX-injected animals entered catagen and telogen, many have lost all MeSCs (Fig. 1e, Telo). Subsequently, when the next round of anagen initiated, differentiated melanocytes were not produced to colour new hair shafts, and unpigmented hairs emerged (Fig. 1e, 2nd Ana, Extended Data Fig. 1h). Although some regenerated hairs remained pigmented, the MeSC numbers in these pigmented hairs were also reduced (Extended Data Fig. 1i). RTX injection led to the same extent of hair greying in both male and female mice (Extended Data Fig. 1j). Moreover, RTX also caused MeSC loss when injected during telogen. In this case, unpigmented hairs appeared as soon as new hairs emerged in the following anagen (Extended Data Fig. 2a, b). These results suggest that MeSCs are exquisitely sensitive to RTX-induced stress, while differentiated melanocytes or melanin synthesis are not directly affected. MeSCs were also lost or reduced in mice subjected to restraint stress or chronic unpredictable stress (Extended Data Fig. 2c). Since stress depleted MeSCs, the loss of hair pigmentation in all three conditions was permanent (Extended Data Fig. 2d). Collectively, these data indicate that stress leads to the loss of MeSCs.

Norepinephrine drives MeSC loss

Next, we asked how stress transmits to the periphery to alter MeSCs (Fig. 2a). Immune attack has been postulated to cause stress-induced hair greying^{2,23}. To test the involvement of the immune system, we injected RTX into Rag1 mutant mice, which lack both T and B cells, and into CD11b-DTR mice, in which myeloid lineages had been ablated by diphtheria toxin. Injection of RTX into these immune-deficient mice still resulted in white hair formation, suggesting that RTX-induced hair greying is independent of T cells, B cells, or myeloid cells (Extended Data Fig. 3a, b).

Since all stressors led to elevated corticosterone and norepinephrine in the blood, we asked if these stress-induced circulating factors played a role in stress-induced MeSC loss. Our RNA sequencing (RNA-seq) data on FACS-purified MeSCs suggested that MeSCs express the glucocorticoid receptor (*GR*, a receptor for corticosterone) and the β 2 adrenergic receptor (*Adrb2*, a receptor for norepinephrine) (Extended Data Fig. 3c, see methods). To determine if GR mediated the effects of stress on MeSCs, we depleted GR in MeSCs using Tyr-CreER^{8,24–26}. RTX injection into Tyr-CreER; *GR* fl/fl animals still resulted in hair greying (Extended Data Fig. 3d). Moreover, no changes in MeSCs or hair pigmentation were observed when corticosterone was elevated via feeding (Extended Data Fig. 3e). These data suggest that corticosterone is not a major driver of stress-induced MeSC loss.

We then explored if ADRB2 might mediate the impact of stress on MeSCs. Upon RTX injection, we observed a marked induction of Phospho-CREB (a downstream effector of ADRB2) in MeSCs but not mature melanocytes (Extended Data Fig. 4a). Moreover, when we depleted ADRB2 from MeSCs using Tyr-CreER, white hairs failed to form following RTX injection (Fig. 2b). These data suggest that ADRB2 expressed by MeSCs is essential for stress-induced hair greying. By contrast, when ADRB2 was depleted from hair follicle stem cells that share the same niche with MeSCs, RTX injection still resulted in hair greying (Extended Data Fig. 4b). In the absence of stress, depletion of ADRB2 in MeSCs did not lead to changes in MeSCs, melanocytes, or pigment production, suggesting that the norepinephrine-ADRB2 pathway is dispensable for melanogenesis during the normal hair cycle (Extended Data Fig. 4c, d). Collectively, these data suggest that norepinephrine signals through ADRB2 on MeSCs to mediate stress-induced hair greying.

To test if elevated norepinephrine was sufficient to cause hair greying in the absence of stress, we introduced norepinephrine locally to the skin via intradermal injections. Local norepinephrine injection promoted hair greying at the injection sites in wild type and in HFSC-specific *Adrb2* knockout mice, but failed to cause hair greying in MeSC-specific *Adrb2* knockout mice (Fig. 2c, Extended Data Fig. 4e–g). Altogether, our data demonstrate that while immune cells and corticosterone are dispensable, norepinephrine signalling appears to be necessary for stress-induced hair greying and sufficient to trigger hair greying in the absence of stress.

Finding the source of norepinephrine

Since the adrenal gland is a major source of norepinephrine under stress, to determine if adrenal gland-derived norepinephrine mediates stress-induced hair greying, we surgically removed both adrenal glands. Adrenalectomy significantly reduced the levels of corticosterone and norepinephrine in the bloodstream of RTX-injected animals (Extended Data Fig. 5a). Yet, injection of RTX into adrenalectomized mice still caused hair greying, suggesting that RTX-induced hair greying is independent of hormones or catecholamines from the adrenal glands (Fig. 2d).

One alternative source of norepinephrine is the sympathetic nervous system. Under stress, the sympathetic nervous system becomes activated to induce fight-or-flight responses through secretion of norepinephrine from peripheral axon terminals¹⁷. In the skin, sympathetic nerves terminate close to the bulge where MeSCs reside (Fig. 3a). Moreover, skin regions with high numbers of unpigmented hairs also have denser sympathetic innervation (Extended Data Fig. 5b).

To determine if sympathetic nerves are indeed activated following RTX injection, we examined levels of c-FOS, an immediate early transcription factor reporting neuronal activity²⁷. Robust c-FOS induction was detected in the cell bodies of sympathetic neurons within 1 hour after RTX injection, peaking around 2–4 hours, and diminishing after 24 hours, suggesting that RTX injection led to a burst activation of sympathetic neurons (Fig. 3b, Extended Data Fig. 5c). Moreover, when buprenorphine was injected together with RTX to block pain, sympathetic neurons failed to induce c-FOS (Fig. 3b, right). These data suggest that the sympathetic nervous system becomes highly activated following nociception-induced stress.

To test if activation of sympathetic nerves is responsible for MeSC loss and hair greying under stress, we ablated sympathetic nerves with 6-hydroxy dopamine (6-OHDA), a selective neurotoxin for sympathetic nerves²⁸. Sympathectomy blocked RTX-induced hair greying and MeSC loss (Fig. 3c, Extended Data Fig. 5d), suggesting that sympathetic nerves indeed mediate stress-induced hair greying. In addition, guanethidine, a chemical that blocks norepinephrine release from sympathetic nerve terminals²⁹, suppressed hair greying and MeSC loss upon RTX injection (Extended Data Fig. 5e). Collectively, these data suggest that norepinephrine secreted from sympathetic nerve terminals mediates the effect of stress on MeSCs.

To determine if sympathetic nerve activation in the absence of stress is sufficient to drive MeSC loss, we took a chemogenetic approach using the Designer Receptor Exclusively Activated by Designer Drugs (DREADDs) system^{3,4}. Gq-DREADD is an artificial Gq-protein coupled receptor activated by the inert molecule Clozapine N-Oxide (CNO) but not by endogenous ligands. Activation of Gq-DREADD leads to intracellular calcium release and neuronal firing. We generated TH-CreER; CAG-*Isl*-Gq-DREADD; Rosa-mT/mG mice, which allowed us to activate sympathetic nerves artificially with CNO (Fig. 3d, Supplementary Discussion). Injection of CNO induced c-FOS activation in sympathetic ganglia, confirming the efficacy of this strategy (Extended Data Fig. 5f). Sympathetic nerve

activation with the DREADD system led to loss of MeSCs and hair greying at the sites where CNO was injected (Fig. 3d, Extended Data Fig. 5g). Moreover, when TH-CreER was activated mosaically by a low dose of tamoxifen, intradermal CNO injection resulted in MeSC loss only in hair follicles innervated by DREADD-positive nerve fibres (recognizable by their membrane GFP expression; Fig. 3e, Extended Data Fig. 5h). These data suggest that sympathetic nerve activation in the absence of stressors is sufficient to drive MeSC loss. Altogether, our findings suggest that elevated norepinephrine secreted from the sympathetic nerve terminals drives MeSC depletion under stress.

Stress drives MeSC hyper-proliferation

Next, we aim to identify the early changes in MeSCs under stress that might account for their loss (Fig. 4a). Immunofluorescence failed to detect active caspase-3 or TUNEL signals in MeSCs before their depletion from the niche upon RTX or norepinephrine injection. Moreover, RTX injection into RIPK3 mutant mice lacking a key kinase for necrosis still caused hair greying (Extended Data Fig. 6a–c). These data suggest stress-induced MeSC loss is not mediated by apoptosis or necrosis. Radiation causes DNA damage in MeSCs, leading to their differentiation within the niche²². However, we failed to detect gamma-H2AX foci (a hallmark of DNA damage) in MeSCs following RTX or norepinephrine injection, suggesting that stress-induced depletion of MeSCs is not mediated through DNA damage (Extended Data Fig. 6d).

Quiescence is a key feature of many somatic stem cells^{30–33}. Loss of quiescence has been postulated to cause MeSC loss in *Bcl2* mutants^{10,34}. To examine if stress alters MeSCs quiescence, we injected RTX or norepinephrine into mice that had entered full anagen, when MeSCs are normally quiescent. We saw a dramatic increase in the number of proliferating MeSCs within 24 hours after RTX or norepinephrine injection—about 50% of MeSCs became positive for Phospho-Histone H3, an M phase marker (Fig. 4b). This number is in sharp contrast to the MeSC proliferation seen in early anagen (~6%), the only stage when MeSCs proliferate to self-renew (Extended Data Fig. 6e)^{9,35}. By contrast, no changes in proliferation or apoptosis were observed in mature melanocytes after RTX or norepinephrine injection (Extended Data Fig. 6f, g). These data suggest that elevated norepinephrine forces MeSCs to enter a rapid and abnormally proliferative state, while sparing mature melanocytes.

To monitor changes in MeSCs following stress, we generated Tyr-CreER; Rosa-mT/mG mice, which allowed us to trace MeSCs by membrane GFP (Fig. 4c). Consistent with the observation that proliferation is an early response of MeSCs to stress, we saw a transient increase in GFP positive cells shortly after RTX injection (Fig. 4c, D1, FACS quantified in Extended Data Fig. 6h). Following this initial phase, many GFP positive cells began to exhibit striking dendritic branching, characteristic of differentiated MeSCs (Fig. 4c, D2). They also began to depart from the bulge—some migrated downwards along the hair follicle, and some migrated out into dermis or epidermis (Fig. 4c, D2 and D3). By Day 3, many GFP positive cells had migrated out of the bulge, and by Day 4, many hair follicles had lost all GFP positive cells in the bulge. Moreover, ectopic pigmentation could be detected along the hair follicle, epidermis, and dermis, places that are normally devoid of

pigments (Fig. 4d, Extended Data Fig. 6i). Collectively, these data suggest that after stress, MeSCs undergo rapid proliferation followed by differentiation and migration, leading to their loss from the niche (Fig. 4e, Supplementary Discussion).

Transcriptome analyses of MeSCs

To discover the molecular mechanisms driving MeSC loss under stress, we conducted RNA-seq using FACS-purified MeSCs from control and RTX-treated animals 12 hours after RTX injection, before MeSCs showed phenotypic differences (Fig. 5a, Extended Data Fig. 7a–c). Examination of marker gene expression for diverse skin cell types confirmed that we had successfully enriched for MeSCs (Extended Data Fig. 7d). To uncover major molecular changes, we conducted Gene Ontology (GO) enrichment analysis (Fig. 5b). We also curated a list of known genes associated with MeSC proliferation and differentiation (Fig. 5c, Extended Data Fig. 7e). Moreover, we utilized a list of genes previously denoted for cell cycle entry to assess if cell cycle regulators are altered at the transcriptional level (Extended Data Fig. 7f)³⁶. Some of these key changes were also verified by quantitative RT-PCR (qRT-PCR) (Extended Data Fig. 7g). Collectively, we identified changes in several cell cycle regulators in stressed MeSCs, including Cyclin-dependent kinase 2 (*Cdk2*), a key promoter of G1 to S transition. Receptors for ligands that promote MeSC proliferation, differentiation, and migration, including *c-Kit*³⁷ and *Mcl1*³⁸, were also upregulated. In addition, genes involved in melanogenesis¹⁹, including *Mitf*, *Tyrp1*, *Tyr*, *Oca2*, and *Pmel*, were upregulated (Fig. 5c, Extended data Fig. 7e, g). These data suggest that MeSCs upregulate proliferation and differentiation programs following stress. Furthermore, norepinephrine exposure also led to a rapid induction of proliferation genes like *Cdk2*, and differentiation genes like *Mitf* and *Tyr* in cultured human melanocyte cells (Fig. 5d). These data suggest that norepinephrine elicits similar responses in both human and mouse melanocyte lineages.

Blocking proliferation preserves MeSCs

Since MeSCs first lose quiescence upon stress, we asked if transient suppression of proliferation early in the stress response might prevent their depletion. For this, we injected RTX at full anagen, and applied CDK inhibitors (AT7519 or Flavopiridol) topically to suppress proliferation transiently until 48 hours post injection^{39,40}. MeSCs in RTX-injected animals treated with CDK inhibitors remained quiescent and were preserved in the niche (Fig. 5e, Extended Data Fig. 8a). Proliferation of cells in the hair bulb remained largely normal, likely because the penetration of inhibitors into subcutaneous regions in full anagen was limited (Extended Data Fig. 8b). To further establish that MeSC loss can be prevented by inhibiting MeSC proliferation, we generated a genetic model (Tyr-CreER; Rosa-lsl-rtTA; TetO-P27) in which the CDK inhibitor P27 can be transiently induced specifically in MeSCs with doxycycline. Induction of P27 expression in MeSCs alone suppressed aberrant MeSC proliferation and preserved MeSCs in the niche under stress (Fig. 5e, Extended Data Fig. 8a). These preserved MeSCs displayed an undifferentiated morphology and retained functionalities, as newly regenerated hairs in subsequent cycles maintained pigmentation (Fig. 5f). Collectively, these data suggest that loss of quiescence drives MeSC depletion in stress, and that suppression of MeSC proliferation is sufficient to prevent their loss.

DISCUSSION

Acute stress is known to cause transient and beneficial “fight-or-flight” responses essential for survival. Here, we demonstrate that acute stress can also cause non-reversible depletion of somatic stem cells through activation of the sympathetic nervous system, resulting in permanent damage to tissue regeneration (Fig. 5g). Our findings support the emerging notion that the sympathetic nervous system not only regulates body physiology, but also influences diverse processes in development and tissue maintenance^{13,41–43}. The adrenal glands are the central regulators of stress responses. However, we show that the adrenal gland-derived circulating stress hormones and catecholamines do not drive changes in MeSCs under stress. Since sympathetic nerves innervate essentially all organs, acute stress might have a broad and rapid impact on many tissues via neuronal signals rather than circulating hormones.

Why does such a nerve-stem cell interaction exist? The connection between the nervous system and pigment-producing cells is likely conserved during evolution. Cephalopods like squid, octopus, or cuttlefish have sophisticated colouration systems that allow them to change colour for camouflage or communication. Neuronal activities control their pigment-producing cells (chromatophores), allowing rapid changes in colour in response to predators or threats⁴⁴. Therefore, an attractive hypothesis is that sympathetic nerves might modulate MeSC activity, melanocyte migration, or pigment production in situations independent of the hair cycle—for example, under bright sunlight or UV irradiation⁴⁵. Under extreme stress, however, hyperactivation of neuronal activities over-stimulates the pathway, driving MeSC depletion.

MeSCs also exhibit ectopic differentiation and depletion with age^{10,20}. Of relevance, patients who have undergone partial sympathectomy develop fewer numbers of unpigmented hairs on the sympathectomized side with age^{46,47}. In the future, it will be interesting to investigate whether the mechanisms we uncover here might also contribute to the MeSC loss during aging, and whether stress might mimic an accelerated aging process.

METHODS

Animals

C57BL/6J, Tyr-CreER, K15-CrePGR, Rag1 mutant, CD11b-DTR, GR flox, CAG-lsl-Gq-DREADD, Rosa-H2BGFP/mCherry, Rosa26-mT/mG, Rosa-lsl-rtTA, and RIPK3 mutant mice were obtained from the Jackson Laboratory. *Adrb2* flox⁴⁸ mice were originally generated by Dr. Gerard Karsenty (Columbia University) and provided to us by Dr. Paul Frenette (Albert Einstein College of Medicine). TH-CreER⁴⁹ mice were generated and provided by Dr. David Ginty (Harvard Medical School). TetO-P27⁵⁰ mice were originally generated by Dr. Gillian K. Cady (Roswell Park Cancer Institute) and provided to us by Dr. Valentina Greco (Yale School of Medicine). All experiments used balanced groups of male and female mice. All experiments are conducted and compared using mice of the same hair cycle stage in comparable age range (P20-P25 for 1st telogen, P31-P36 for full anagen, and P50-P60 for 2nd telogen, or long-term monitoring as specified). To monitor hair cycle, mice were shaved at weaning to monitor skin colour changes and confirmed by skin sections. The

acquisition of human melanocyte cells was carried out in compliance with the IRB policies at MGH. All animals were maintained in an Association for Assessment and Accreditation of Laboratory Animal Care-approved animal facility at Harvard University, Harvard Medical School, and Ribeirao Preto Medical School. Procedures were approved by the Institutional Animal Care and Use Committee of all institutions and were in compliance with all relevant ethical regulations.

Stress procedures

Restraint and chronic unpredictable stress (CUS) procedures were performed as previously described^{11–14}. Briefly, for restraint stress, C57BL/6J mice were kept in a restrainer (Fisher Scientific 12972590) for 4 hours a day for five days starting from mid-anagen (P28-P30). Hairs were depilated to induce hair regeneration when their hair cycle reached telogen. Mice were depilated 4 times in total to monitor long-term changes. For CUS, C57BL/6J mice were exposed to a combination of stressors. Two of the stressors were applied each day. The stressors include cage tilt, isolation, damp bedding, rapid light/dark changes, overnight illumination, restraint, empty cage, and 3x cage change. All stressors were randomly repeated in consecutive weeks.

Drug treatments

For RTX injection (see also Supplementary Discussion), mice received injections of RTX (30–100 µg/kg) in the flank for 1–3 days as described previously^{15,16,51–56}. RTX was prepared in 2% DMSO with 0.15% Tween 80 in PBS. Control mice were treated with the vehicle only. RTX injection was done either in full anagen (P31-P36) or in 1st telogen (P21). For corticosterone feeding, 35 µg/ml corticosterone (Millipore Sigma, C2505) was dissolved in 0.45% hydroxypropyl-β-cyclodextrin and provided in drinking water. Mice were treated for three days (P28-P30). Control mice received the vehicle water (0.45% β-cyclodextrin). For analgesia, mice were injected with buprenorphine (0.1 mg/kg) 4 hours before RTX injection, and every 6 hours after RTX injection for 2 days. For tamoxifen treatment, tamoxifen was diluted in corn oil to a final concentration of 20 mg/ml. To induce recombination, 20 mg/kg was injected intraperitoneally once per day for 4–7 days. For mosaic induction of Tyr-CreER and TH-CreER, 20 mg/kg tamoxifen was injected intraperitoneally once per day for 3 days. For intradermal norepinephrine injection, norepinephrine (Sigma-Aldrich 489350) solution was prepared freshly by dissolving in 0.1% ascorbic acid in 0.9% sterile NaCl to a final concentration of 2 mM. 50 µl was injected intradermally into experimental animals together with fluorescent beads at full anagen (P31~P36). Control animals were injected with equivalent volume of vehicle (0.1% ascorbic acid in 0.9% sterile NaCl) with fluorescent beads. The injection sites were marked using water resistant ink. For sympathetic nerve ablation, 6-hydroxydopamine hydrobromide (6-OHDA, Sigma 162957) solution was prepared freshly by dissolving 6-OHDA in 0.1% ascorbic acid in 0.9% sterile NaCl. 100 mg/kg (body weight) of 6-OHDA was injected intraperitoneally daily from P18 to P22. Control animals were injected with equivalent volume of vehicle (0.1% ascorbic acid in 0.9% sterile NaCl). Ablation efficiency in the skin was confirmed by immunofluorescence staining. For guanethidine treatment, mice were intraperitoneally injected with 30 mg/kg (body weight) of guanethidine (Sigma-Aldrich, 1301801), once a day for 3 consecutive days prior to RTX administration at full anagen

(P31~P36). For Induction of Gq-DREADD, 50 μ l CNO (1 mg/ml in 0.9% sterile saline) was injected intradermally into experimental animals together with fluorescent beads at full anagen (P31~P36). Control animals were injected with equivalent volume of vehicle (0.9% sterile saline) together with fluorescent beads. For diphtheria toxin administration, diphtheria toxin (DT, Sigma-Aldrich) was dissolved in 0.9% saline (0.1 mg/ml). For ablation, CD11b-DTR transgenic mice were intraperitoneally injected with 25 ng/g (body weight) DT daily 3 days before RTX injection at full anagen (P31~P36). 20 ng/g (body weight) DT was injected every three days after RTX injection until harvesting. For inhibitor treatment, mice were shaved and pre-treated with 5 mg/kg (body weight) AT7519 (Cayman Chemical 16231) or Flavopiridol (Cayman Chemical 10009197) in ethanol topically 48 hours and 24 hours before RTX injection, at the time of RTX injection, and 24 hours and 48 hours after injection. For P27 expression induction, mice were fed with Doxycycline Rodent Diet (VWR 89067–462) for three days before the RTX treatment and three days after. RTX was given at Anagen VI (P31~P36).

Quantification of unpigmented hairs

For Restraint and CUS, unpigmented hairs were quantified by plucking ~100 hairs from 3–4 regions of the skin across the anterior to posterior end, and the percentage of white hairs were calculated by dividing the number of white hairs by the total number of hairs plucked. For RTX injection experiments, the percentage of white hair regions was calculated by dividing the size of white hair areas with the size of the whole skin (both areas were measured using ImageJ). For intradermal injection experiments (NE or CNO), unpigmented hairs were quantified by plucking ~100 hairs from each injection site (marked by water resistant ink at the time of injection), and the percentage of white hairs were calculated by dividing the number of white hairs by the total number of hairs plucked.

Histology and immunohistochemistry

Mouse skin samples were fixed using 4% paraformaldehyde (PFA) for 15 minutes at room temperature, washed 6 times with PBS, and immersed in 30% sucrose overnight at 4°C. Samples were then embedded in OCT (Sakura Finetek). 35~50 μ m sections were fixed in 4% paraformaldehyde (PFA) for 2 minutes and washed with PBS and PBST. Slides were then blocked using blocking buffer (5% donkey serum; 1% BSA, 2% cold water fish gelatin in 0.3% Triton in PBS) for 1 hour at room temperature, followed by staining with primary antibodies overnight at 4°C and secondary antibody for 4 hours at room temperature. For sympathetic nerve density quantification, 90 μ m sections were used. EdU was developed for 1 hour using the Click-It reaction according to manufacturer instructions (Thermo Fisher Scientific). TUNEL assay was performed according to manufacturer instructions (Roche). Fontana–Masson staining was performed according to manufacturer instructions (Market Lab ML7255). Antibodies used: TRP2 (Santa Cruz 10451, 1:800), tyrosine hydroxylase (rabbit, Millipore AB152, 1:1000 or sheep, Millipore AB1542, 1:150–1:300), c-Fos (Abcam, 190289, 1:1000), γ -H2AX (Cell Signaling, 9718, 1:400), phospho-histone H3 (rabbit, Cell Signaling Technology 3377S, 1:500), cleaved caspase 3 (rabbit, Cell Signaling Technology 9664S, 1:400), GFP (rabbit, Abcam ab290, 1:1000 or chicken, Aves labs GFP-1010, 1:200), CD3 (eBioscience 14–0032-81, 1:800), CD11b (eBioscience 14–

0112-81, 1:800), Phospho-CREB (Cell Signaling 9198, 1:800), MITF (Abcam ab12039, 1:400).

Measurement of stress hormones

50 μ l of blood plasma was collected from each mouse and transferred into a 1.5 ml microcentrifuge tube. 10 μ l of internal solution was added to each sample followed by 100 μ l of water and 640 μ l of methanol. Samples were incubated at -20°C for 1 hour, then centrifuged 30 minutes at maximum speed at -9°C . The supernatant was transferred to a new tube and dried under N_2 flow and resuspended in 50 μ l methanol and transferred to micro-inserts. All samples were run on an Agilent 6460 Triple Quad LC/MS with an Agilent 1290 Infinity HPLC. For corticosterone-treated mice, plasma corticosterone levels were determined by ELISA according to the manufacturer's instruction (Arbor Assays, K014-H1).

Radiation

Ten-week-old C57BL/6J mice were gamma irradiated (^{137}Cs source) with a split 10.5 gray split dose. Mice were transplanted with 300,000 whole bone marrow cells to ensure survival after lethal irradiation.

FACS

Mouse dorsal skin was collected, and the fat layer was removed by gentle scrapping from the dermal side. The skin was incubated in 0.25% collagenase in HBSS at 37°C for 35–45 minutes on an orbital shaker. Single cell suspension was collected by gentle scraping of the dermal side and filtering through 70 μm and 40 μm filters. The epidermal layer was incubated in trypsin-EDTA at 37°C for 35–45 minutes on an orbital shaker. Single cell suspension was collected by gentle scraping of the epidermal side and filtering through 70 μm and 40 μm filters. The single cell suspension was centrifuged for 5 minutes at 4°C , resuspended in 0.25% FBS in PBS, and stained with fluorescent dye-conjugated antibodies for 30 minutes. For late anagen skin samples, the bottom parts of the hair follicles containing mature melanocytes were removed by gentle scrapping under dissection microscope. The MeSCs located close to the bulge remained and were verified by immunostaining. Antibodies used: CD140a (Invitrogen 13–1401-82, 1:200), CD45 (Invitrogen 13–0451-82, 1:400), Sca1 (Invitrogen 13–5981-82, 1:1000), CD34 (Invitrogen 13–0341-82, 1:100), CD117 (Biolegend 135136, Dilution 1:400). See a protocol published at protocol exchange website for a step-to-step instruction⁵⁷.

RNA isolation

RNA was isolated using a RNeasy Micro Kit (Qiagen), using QIAcube according to manufacturer instructions. RNA concentration and RNA integrity were determined by Bioanalyzer (Agilent, Santa Clara, CA) using the RNA 6000 Nano chip. High quality RNA samples with RNA Integrity Number ≥ 8 were used as input for RT-PCR and RNA-sequencing.

Cell Culture

Primary human melanocytes were derived from neonatal foreskin as previously described⁵⁸ and cultured in Medium 254 (Invitrogen, Thermo Fisher Scientific). Melanocytes (passages 2 and 4) were starved for 24 hours in HAM's F-10 + 1% penicillin/streptomycin/glutamine before adding NE (10uM).

Quantitative real-time PCR

The cDNA libraries were synthesized using Superscript IV VILO master mix with ezDNase (Thermo Fisher). Quantitative real time PCR was performed using power SYBR green (Thermo Fisher) in an ABI QuantStudio6 Flex qPCR instrument. Ct values were normalized to an internal control of beta-actin.

Imaging and image analysis

All images were acquired using a Zeiss LSM 880 confocal microscope or Keyence microscope using x20 or x40 magnification lenses. Images are presented as Maximum Intensity Projection images. For colocalization analysis, images are presented as a single Z stack. For sympathetic nerve density quantification, TH staining of sympathetic nerves was performed on 90 uM thick skin section samples to ensure the capture of all fibres innervating each hair follicle. Sympathetic nerves innervating individual hair follicles were selected and imaged using a Zeiss LSM 880 confocal microscope. 3D surfaces of TH staining were created using Imaris x64 9.3.0 software and the volume was measured and compared. To quantify cell numbers (MeSC numbers, cell death events, proliferation events) within a hair follicle, immunofluorescence staining images of skin sections from multiple regions across the body were used. The number of cells were counted manually or by using ImageJ.

Statistical analysis

Statistical analyses were performed with Prism 7.00 using unpaired two-tailed Student's t-test, One-Way or Two-Way ANOVA. All statistical tests performed are indicated in the figure legends. The data are presented as mean \pm SD.

RNA-seq and computational analysis

MeSCs were purified using FACS from control and stressed mice skin samples at telogen based on their expression of CD117⁷, starting from a population that is negative for CD140a, CD45, Sca1, and CD34⁵⁷. 2 ng of total RNA from each sample were used to generate RNA-seq libraries using a SMART-Seq v4 Ultra Low Input RNA kit (Takara, 634888) and Nextera XT DNA Library Preparation Kit (Illumina, FC-131-1024). Single-end sequencing reads were obtained using Illumina NextSeq 500 platform. Sequencing reads from RNA-seq libraries were trimmed using Trim Galore! (https://www.bioinformatics.babraham.ac.uk/projects/trim_galore/) and aligned to the mouse reference genome (mm10) using STAR aligner⁵⁹. Reads with alignment quality < Q30 were discarded. Gene expression levels were normalized and differential genes were calculated using DEseq2 package in R⁶⁰. Gene set functional enrichment analysis was performed using David^{61,62}. Transcripts Per Kilobase Million (TPM) calculated from count tables of Control MeSC samples were used to

determine the expression levels of adrenergic receptors and glucocorticoid receptor shown in Fig. 2c.

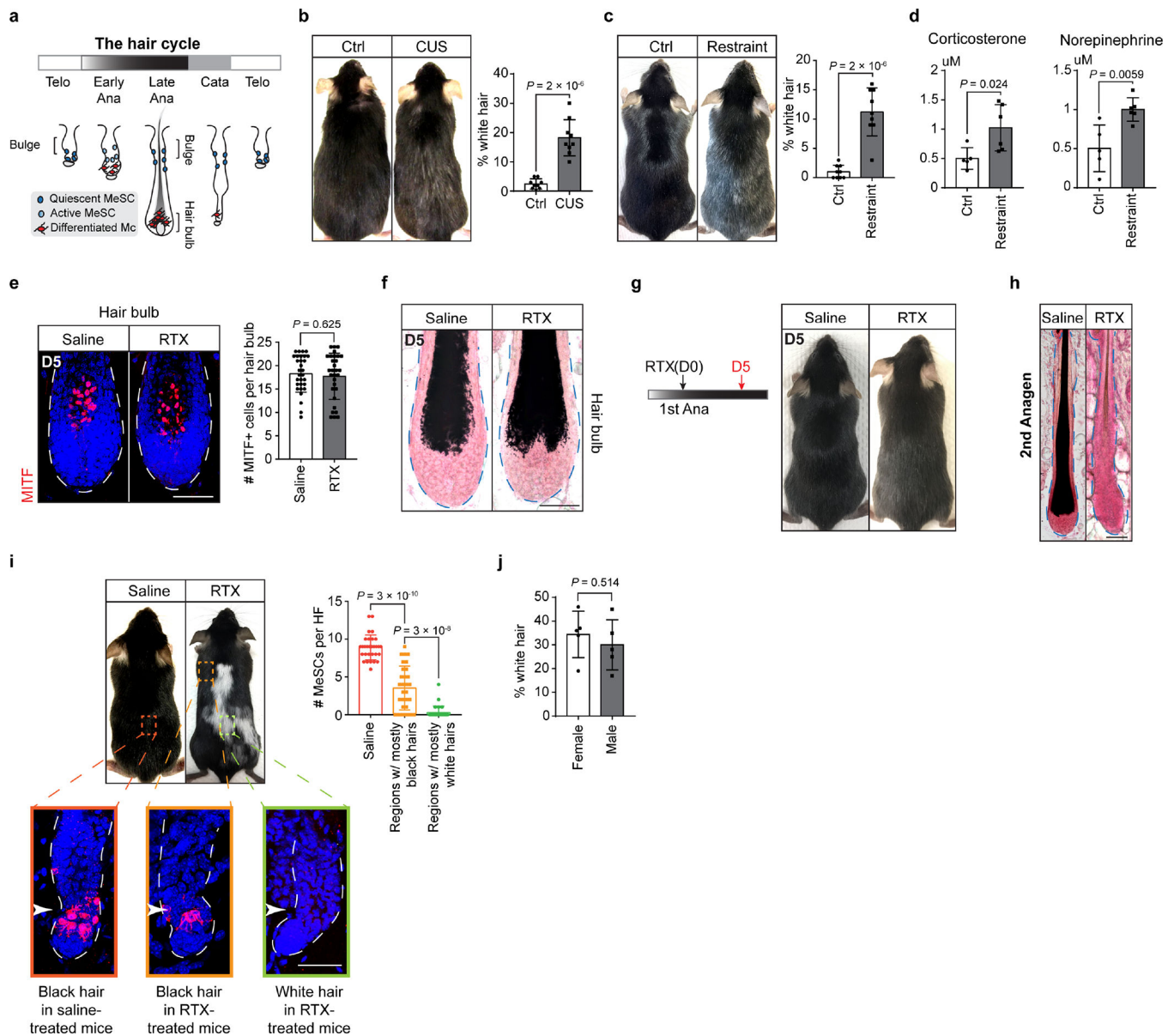
Extended Data

Author Manuscript

Author Manuscript

Author Manuscript

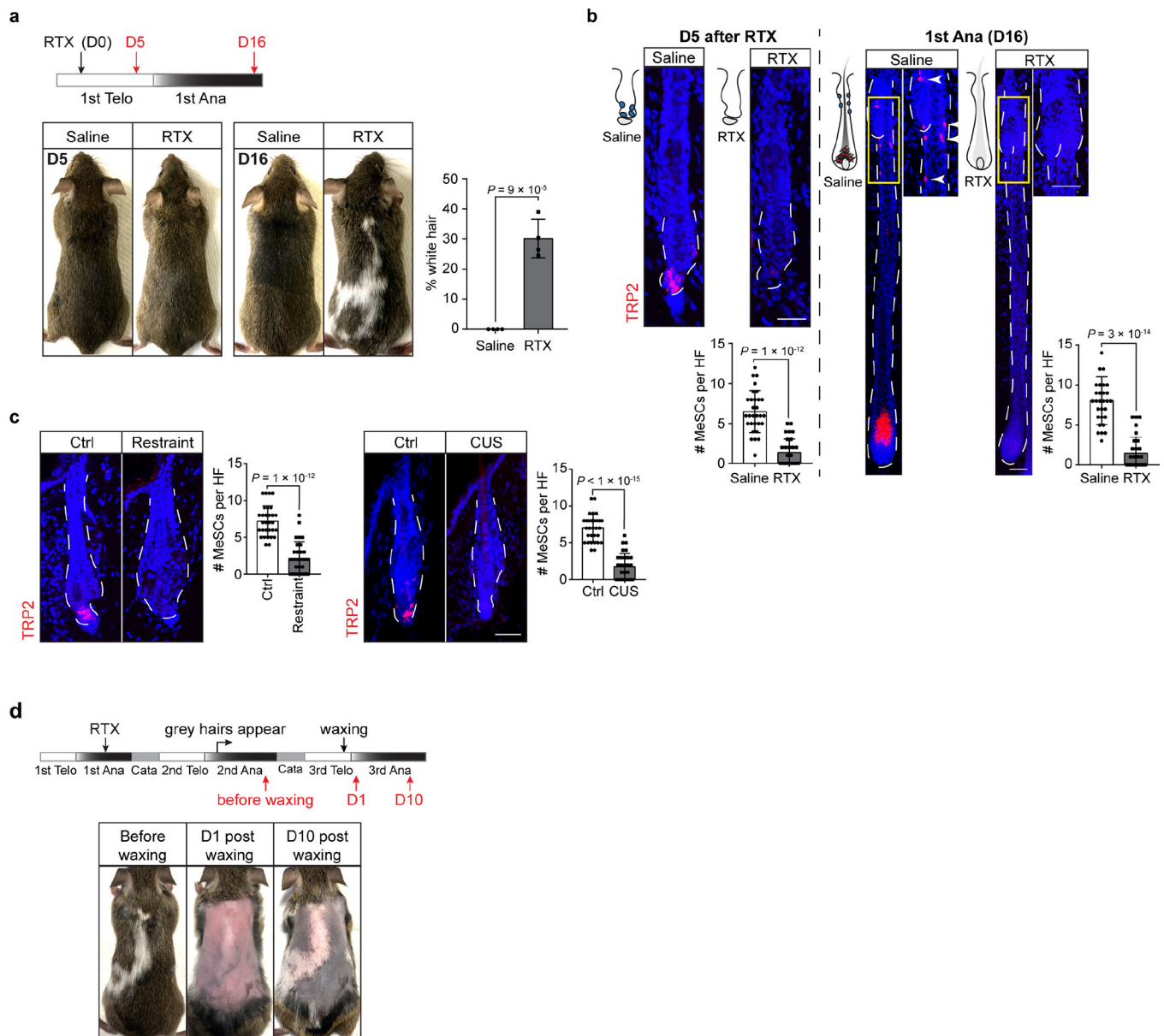
Author Manuscript



Extended Data Fig. 1 | Effects of stress on the hair pigmentation.

a, Schematic of MeSC behaviour during hair cycle. **b**, Hair greying after mice are subjected to chronic unpredictable stress (CUS). Quantifications are done by plucking ~100 hairs from different regions across the skin and counting the number of white hairs ($n = 9$ plucked regions from 3 mice for each condition, two-tailed unpaired t -test). **c**, Hair greying after mice are subjected to restraint stress. Quantifications are done as described in **b**. **d**, LC-MS-MS quantification of corticosterone and norepinephrine after restraint stress ($n = 5$ mice for control and $n = 6$ mice for restraint, two-tailed unpaired t -test). **e**, Immunofluorescent staining of hair bulbs for Melanocyte Inducing Transcription Factor (MITF, red) from mice 5 days after treatment of saline or RTX ($n = 30$ HF from 3 mice for each condition, two-tailed unpaired t -test). **f**, Fontana–Masson staining of hair bulbs for melanin from mice 5 days after treatment of saline or RTX ($n = 6$ mice for each condition). **g**, Hair coat colour in mice 5

days after RTX injection in anagen. RTX is injected in full anagen and the mice are examined 5 days later at late anagen. The coat colour remains black ($n = 6$ mice for each condition). **h**, Fontana–Masson staining of HFJs for melanin from mice treated with saline or RTX at first anagen and examined at second anagen (see Fig. 1e, 2nd Ana for corresponding fluorescent images, $n = 6$ mice for each condition). **i**, Quantification of MeSC numbers in saline and RTX-injected skins. For the RTX-injected skins, the number of MeSCs in regions with predominantly black hairs and regions with many white hairs are quantified separately. Orange and green dashed boxes denote representative black and white hair regions in RTX injected mice. Enlarged boxes contain representative immunofluorescent images of HFJs from each region. White arrowheads indicate regions where MeSC reside. $n = 30$ HFJs from 3 mice for each condition, one-way ANOVA with Tukey's multiple comparisons. **j**, Quantification of the body area covered by white hairs in female vs. male mice ($n = 5$ mice for each sex, two-tailed unpaired t -test). All data are mean \pm S.D.



Extended Data Fig. 2 | Loss of MeSCs after three different stress models.

a, Upper panel, schematic of experimental design for RTX injection in first telogen (red arrows indicate harvesting). Lower panel left, representative mouse images 5 days and 16 days after RTX injection in first telogen. Lower panel right, quantification of the body area covered by white hairs 16 days after RTX injection ($n = 4$ mice for each condition, two-tailed unpaired t -test). **b**, Immunofluorescent staining for TRP2 from saline or RTX-injected mice ($n = 30$ HF from 4 mice for each condition, two-tailed unpaired t -test). Yellow boxes denote the upper HF region where MeSCs reside. Enlarged view of the yellow box regions are shown to the right. Arrowheads indicate MeSCs. **c**, Immunofluorescent staining for TRP2 (red) from mice subjected to CUS or restraint stress ($n = 30$ HF from 5 mice for each condition, two-tailed unpaired t -test). **d**, Hair coat colour is monitored in RTX-injected mice for multiple rounds of hair follicle regeneration (waxing is used to initiate new rounds of

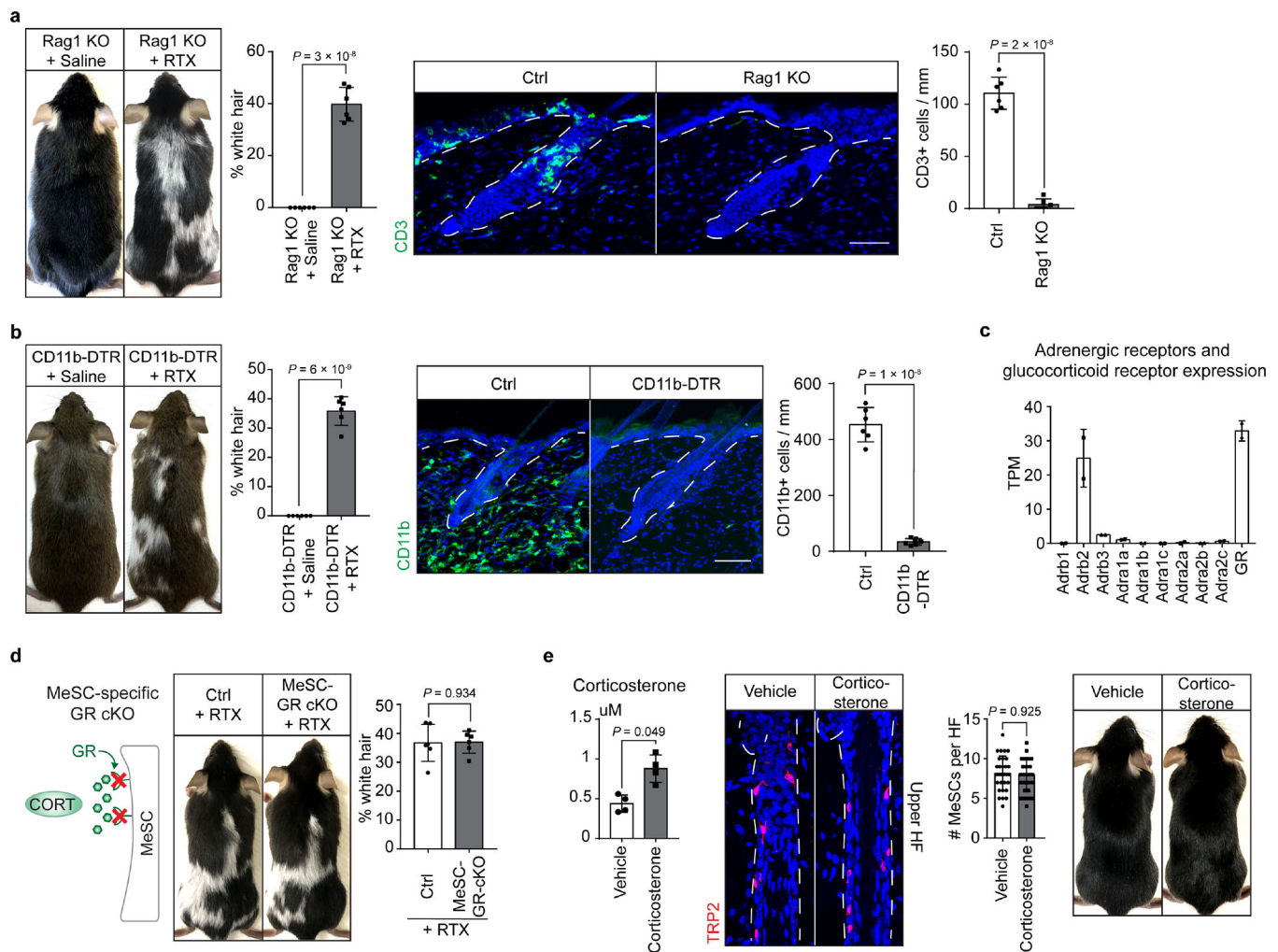
anagen, n = 3 mice for each condition). Schematic denotes the experimental design. Scale bars, 50 μ m. All data are mean \pm S.D.

Author Manuscript

Author Manuscript

Author Manuscript

Author Manuscript



Extended Data Fig. 3 | Stress-induced hair greying is not mediated through corticosterone or immune attack.

a, Left, white hair formation after RTX injection in Rag1 mutant mice devoid of T and B cells (Rag1 KO, $n = 6$ for each condition, two-tailed unpaired t -test). Right, immunofluorescent staining for T cell marker CD3 (green) in control and Rag1 KO skin ($n = 6$ mice for each condition, two-tailed unpaired t -test). **b**, Left, hair greying occurs when RTX is injected into CD11b-DTR mice treated with diphtheria toxin (DT) to deplete myeloid cells ($n = 6$ mice for each condition). Right, immunofluorescent staining for CD11b (green) in DT treated control and CD11b-DTR skin ($n = 6$ mice for each condition). **c**, Expression of adrenergic receptors and glucocorticoid receptor (GR) in MeSCs ($n = 2$ biologically independent samples). **d**, White hair formation following RTX injection into Tyr-CreER; *GR* fl/fl mice (MeSC-GR cKO; $n = 6$ mice for each condition, two-tailed unpaired t -test). **e**, Left, enzyme-linked immunosorbent assay (ELISA) measurement of corticosterone level in the blood 3 days after supplying corticosterone in drinking water ($n = 4$ mice for each condition). Middle, immunofluorescent staining of hair follicles for TRP2 (red) from mice 5 days after corticosterone treatment ($n = 30$ HF from 3 mice for each condition, two-tailed unpaired t -test). Right, hair coat colour after HF in corticosterone-treated mice enter

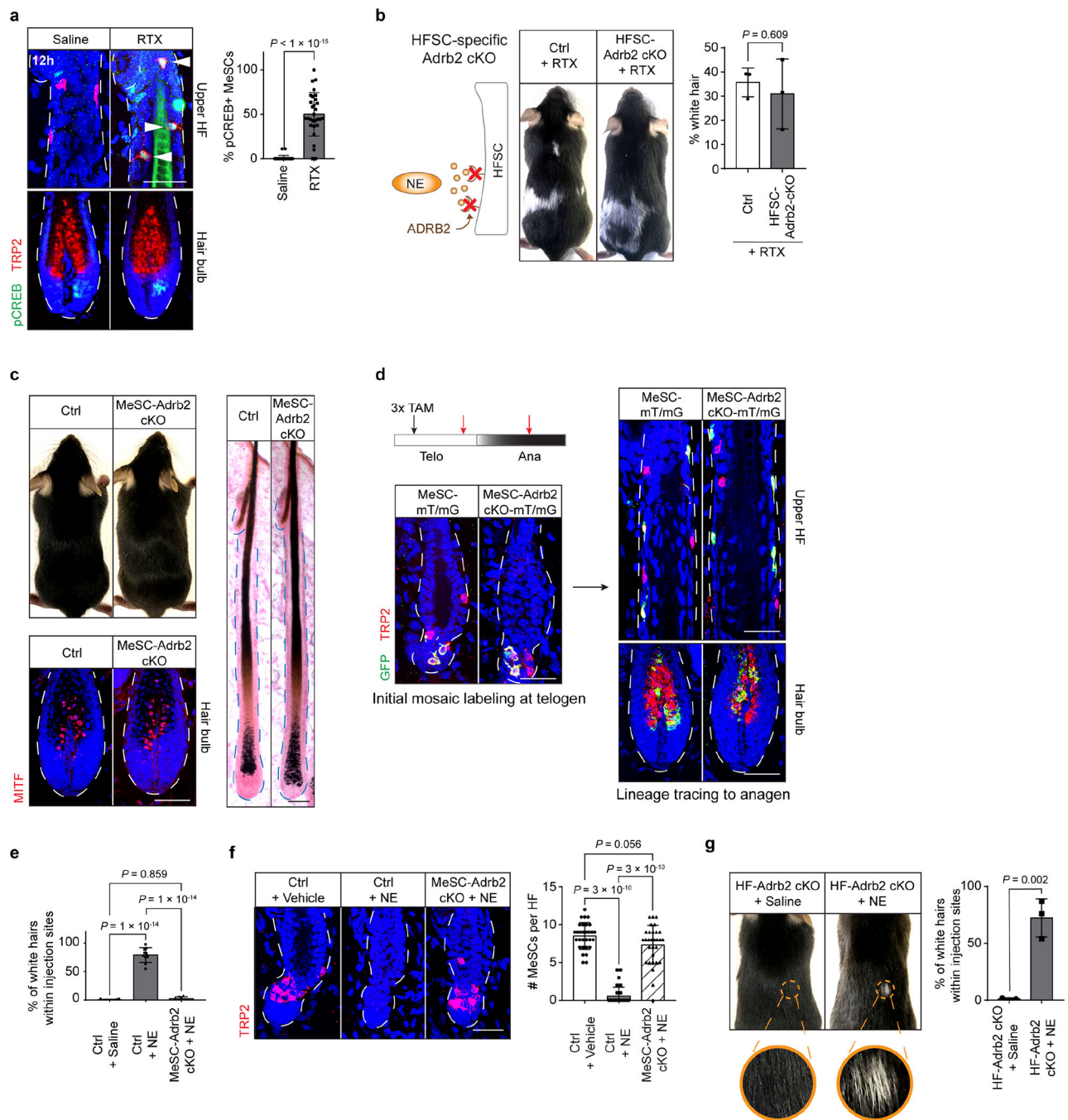
another round of anagen to regenerate new hairs. CORT: corticosterone. Scale bars, 50 μm .
All data are mean \pm S.D.

Author Manuscript

Author Manuscript

Author Manuscript

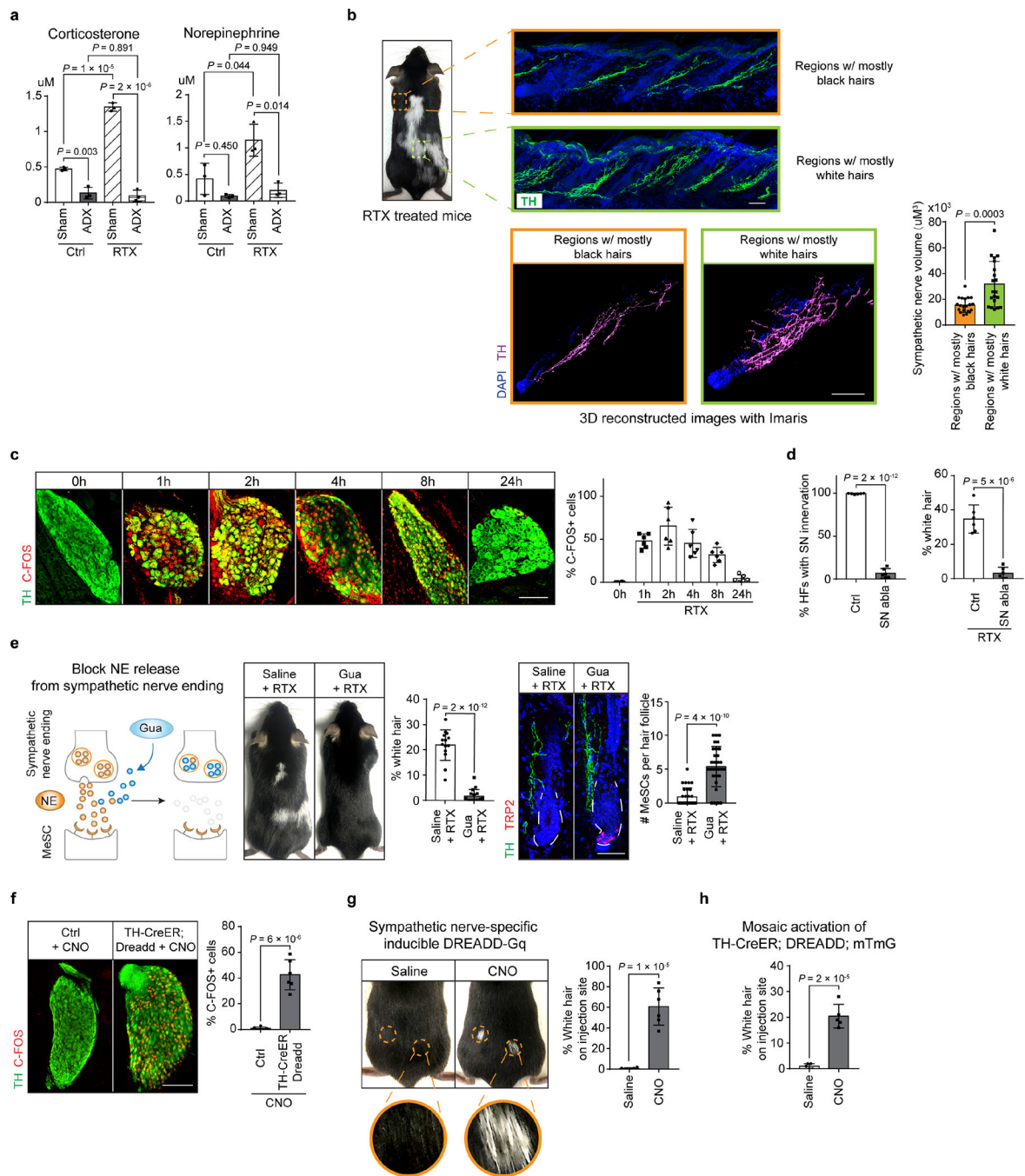
Author Manuscript



Extended Data Fig. 4 | Perturbations of the norepinephrine-ADRB2 pathway.

a, Immunofluorescent staining of HF sections for Phospho-CREB (green) and TRP2 (red) 12 hours after RTX injection ($n = 30$ HF sections from 3 mice for each condition, two-tailed unpaired t -test). White arrowheads indicate Phospho-CREB positive MeSCs in upper HF sections after RTX injection. **b**, White hair formation following RTX injection into K15-CrePGR; *Adrb2* fl/fl mice (HFSC-*Adrb2* cKO; $n = 3$ mice for each condition, two-tailed unpaired t -test). **c**, Upper left, hair coat colour in unstressed Tyr-CreER; *Adrb2* fl/fl mice (MeSC-*Adrb2* cKO) in the second telogen after 7x tamoxifen treatment at the first telogen. Lower left,

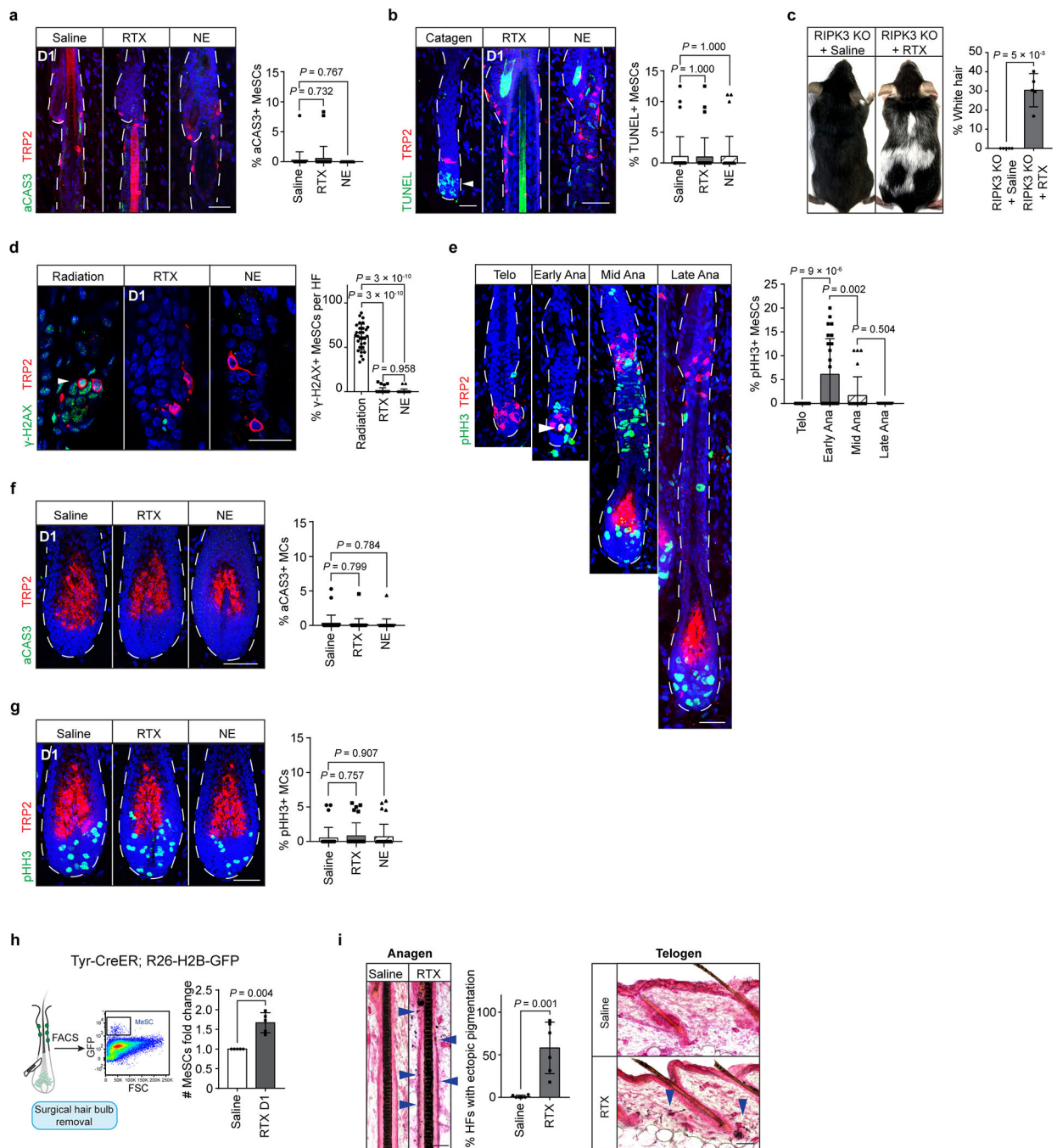
immunofluorescent staining of hair bulbs for MITF (red) in Tyr-CreER; *Adrb2* fl/fl mice in anagen. Right, Fontana–Masson melanin staining of anagen HF from Tyr-CreER; *Adrb2* fl/fl mice (n = 3 mice for each condition). **d**, Upper left, schematic of experimental design for mosaic labelling in unstressed control and *Adrb2* knockout (red arrows indicate harvesting). Lower left, immunofluorescent staining for GFP (green) and TRP2 (red) from Tyr-CreER; R26-mT/mG mice (MeSC-mT/mG) and Tyr-CreER; *Adrb2* fl/fl; R26-mT/mG mice (MeSC-*Adrb2* cKO-mT/mG) after 3x tamoxifen treatment at first telogen. Right, immunofluorescent staining of HF for GFP (green) and TRP2 (red) after the mice enter anagen (n = 3 mice for each condition, TAM: tamoxifen). **e**, Quantification of white hair percentage after intradermal injection of saline or norepinephrine (n = 10 injected sites from 6–8 mice for each condition, one-way ANOVA with Tukey’s multiple comparisons). **f**, Immunofluorescent staining of HF for TRP2 (red) from mouse skins intradermally injected with NE (n = 30 HF from 10 injection sites for each condition, one-way ANOVA with Tukey’s multiple comparisons). **g**, White hairs are formed after intradermal injection of NE in K15-CrePGR, *Adrb2* fl/fl mice (HF-*Adrb2* cKO, n = 3 injection sites for each condition, two-tailed unpaired *t*-test). Yellow dashed circles denote intradermal injection sites. Scale bars, 50 μ m. All data are mean \pm S.D.



Extended Data Fig. 5 | Activation of the sympathetic nervous system by nociception-induced stress or sympathetic nerve-specific inducible Gq-DREADD.

a, LC-MS-MS quantification of stress hormones in sham-operated and adrenalectomized mice (ADX, $n = 3$ mice for each condition, two-way ANOVA with original FDR method of Benjamini and Hochberg). **b**, Upper panel, immunofluorescent staining of sympathetic nerves in the skin regions with predominantly black hairs (orange box) and regions with mostly white hairs (green box, $n = 3$ mice for each condition). Lower panel, 3D surfaces of TH staining created using Imaris software and quantification of sympathetic nerve volume

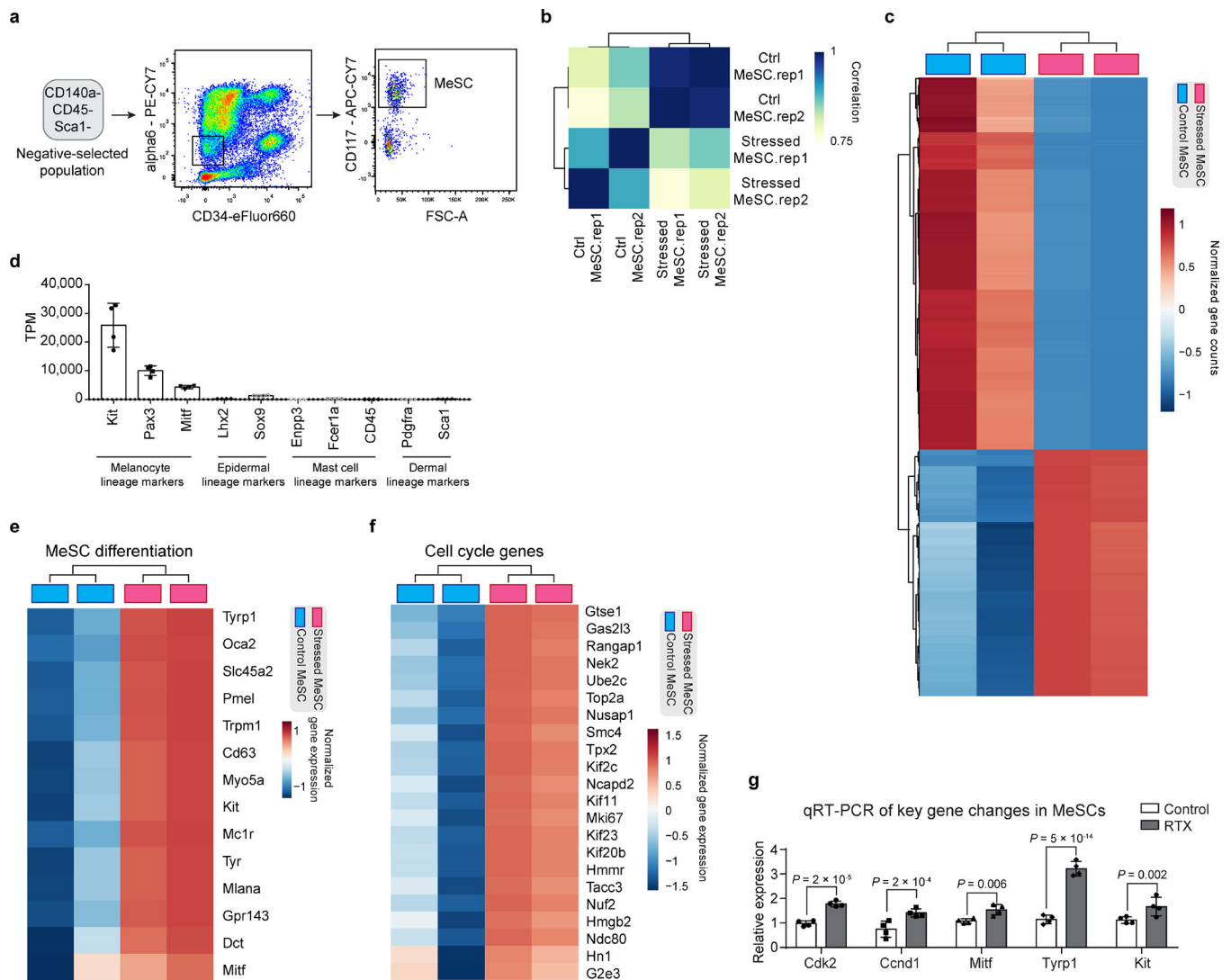
from regions with different number of unpigmented hairs ($n = 20$ HFs for each region from 3 mice, two-tailed unpaired t -test). **c**, Immunofluorescent staining of sympathetic ganglia for TH (green) and c-FOS (red) from mice injected with RTX and harvested at different time points between 0 to 24 hours ($n = 6$ sympathetic ganglia from 3 mice for each time points). **d**, Quantification of chemical sympathectomy efficiency ($n = 6$ mice for each condition, two-tailed unpaired t -test) and % of white hairs in RTX-injected mice treated with vehicle or 6-OHDA ($n = 6$ mice for each condition, two-tailed unpaired t -test). **e**, Guanethidine (Gua) injection blocks formation of white hairs induced by RTX injection (quantification for % of white hairs: $n = 14$ mice for each condition, two-tailed unpaired t -test; quantification for MeSC numbers: $n = 30$ HFs from 6 mice for each condition, two-tailed unpaired t -test). **f**, Immunofluorescent staining of sympathetic ganglia for TH (green) and c-FOS (red) from TH-CreER; Gq-DREADD mice injected with CNO and harvested 6 hours later ($n = 6$ sympathetic ganglia from 2 mice for each condition, two-tailed unpaired t -test). **g**, White hair formation after intradermal injection of CNO into TH-CreER, Gq-DREADD mice ($n = 6$ injection sites from 5 mice for each condition, two-tailed unpaired t -test). Yellow dashed circles denote intradermal CNO injection sites. **h**, Quantification of white hair percentage on CNO injection sites in mosaically-induced TH-CreER; Gq-DREADD; R26-mT/mG mice ($n = 5$ injection sites from 4 mice for each condition, two-tailed unpaired t -test). Scale bars, 50 μm . All data are mean \pm S.D.



Extended Data Fig. 6 | Apoptosis and proliferation analysis of MeSCs and the impact of RTX or norepinephrine on mature melanocytes.

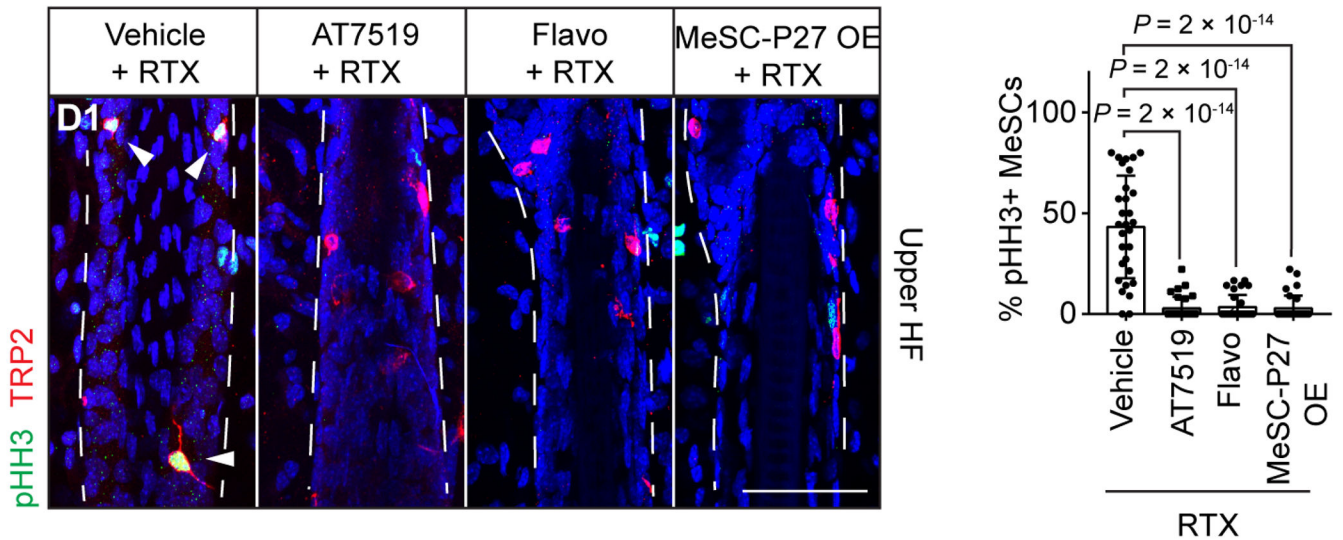
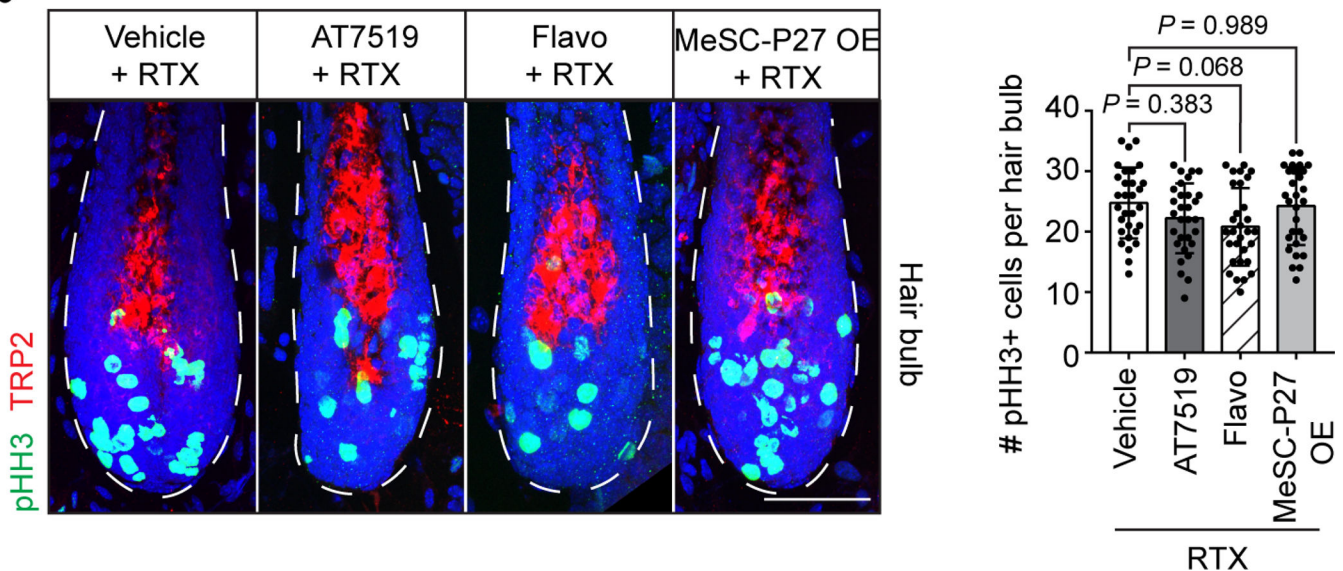
a, Immunofluorescent staining of active Caspase3 (aCAS3, green) and TRP2 (red) from mice 1 day after RTX or NE injection ($n = 30$ HF from 6 mice for each condition, one-way ANOVA with Tukey's multiple comparisons). **b**, Terminal deoxynucleotidyl transferase dUTP nick end labelling (TUNEL) assay of HF from mice 1 day after RTX or NE treatment. Catagen HF are used as positive controls for TUNEL. White arrowhead points to apoptotic hair follicle cells ($n = 30$ HF from 6 mice for each condition, one-way ANOVA

with Tukey's multiple comparisons). **c**, White hair formation in RIPK3 mutant mice (RIPK3 KO) injected with RTX (n = 5 mice for each condition, two-tailed unpaired *t*-test). **d**, Immunofluorescent staining of HFJs for the DNA damage marker γ -H2AX (green) and TRP2 (red) from mice 1 day after RTX or NE treatment. HFJs from irradiated mice are used as positive controls. White arrowhead indicates the MeSCs with DNA damage (n = 30 HFJs from 6 mice for each condition, one-way ANOVA with Tukey's multiple comparisons). **e**, Immunofluorescent staining for pHH3 (green) and TRP2 (red) of control HFJs at different hair cycle stages (n = 25 HFJs from 3 mice for each condition, one-way ANOVA with Tukey's multiple comparisons). **f**, Immunofluorescent staining of hair bulbs for aCAS3 (green) and TRP2 (red) from mice 1 day after RTX or NE injection (n = 30 HFJs from 3 mice for each condition, one-way ANOVA with Tukey's multiple comparisons). **g**, Immunofluorescent staining of hair bulbs for pHH3 (green) and TRP2 (red) from mice 1 day after RTX or NE injection (n = 30 HFJs from 3 mice for each condition, one-way ANOVA with Tukey's multiple comparisons). **h**, Left panel, schematic of MeSCs isolation strategy. Right panel, FACS analysis of MeSC numbers 1 day after RTX (n = 5 mice for each condition, two-tailed unpaired *t*-test). **i**, Fontana–Masson melanin staining of anagen or telogen samples 5 days after saline or RTX injection (n = 6 mice for each condition, two-tailed unpaired *t*-test). Blue arrowheads indicate ectopic pigments. Scale bars, 50 μ m. All bar graphs are mean \pm S.D.



Extended Data Fig. 7 | Differential gene expression in normal and stressed MeSCs.

a, FACS strategy for MeSCs purification. MeSCs are selected based on their expression of CD117, from a population that is negative for CD140a, CD45, Sca1, CD34, and modest expression for Integrin alpha-6. **b**, Sample clustering based on Pearson's correlation of transcriptome among control and stressed MeSCs ($n = 2$ biologically independent samples for each condition). **c**, Heatmap of all differentially expressed genes ($n = 2$ biologically independent samples for each condition, P values calculated using Wald test implemented in DESeq2, and adjusted using the Benjamini–Hochberg method. Log₂FoldChange > 0.58 and adjusted p value < 0.05). **d**, Expression level of marker genes for different cell types in the skin confirming the purity of MeSCs used for RNA-seq ($n = 4$ biologically independent samples). **e**, Heatmaps showing expression of signature genes related to MeSC differentiation. **f**, Heatmaps illustrating expression of cell cycle signature genes. **g**, qRT-PCR validation of selected differentially expressed genes in FACS-purified mouse MeSCs from control and RTX injected skins ($n = 4$ biological replicates for each condition, two-way ANOVA with original FDR method of Benjamini and Hochberg). All data are mean \pm S.D.

a**b**

Extended Data Fig. 8 | Proliferation analysis of RTX-injected mice treated with CDK inhibitors chemically or genetically.

a-b, Immunofluorescent staining of upper HF and hair bulbs for pHH3 (green) and TRP2 (red) from mice 1 day after RTX injection together with topical application of CDK inhibitors (AT7519 or Flavopiridol) or with MeSC-specific P27 overexpression (MeSC-P27 OE, $n = 30$ HF from 3 mice for each condition, one-way ANOVA with Tukey's multiple comparisons). Scale bars, 50 μm . All data are mean \pm S.D.

Supplementary Material

Refer to Web version on PubMed Central for supplementary material.

ACKNOWLEDGEMENTS

We thank G. Karsenty for *Adrb2* fl/fl mice, D. Ginty for TH-CreER mice, and many colleagues who generously donated mice to JAX; A. Wagers, W. Anderson, C-Y Chang, Y. Fong, Q. Ma, M. Nahrendorf, A. Sahay, and members of the Hsu lab in particular M. Gonzalez-Celeiro for discussions and comments on the manuscript, S. Kim, Y-L. Kang, and O. Chung for technical assistance; HCBI, HSCRFB FACS core, histology core, FAS Small Molecule Mass Spectrometry Facility, Office of Animal Resources, and the Bauer Core Facility at Harvard University for technical support; This work was supported in part by the Harvard Stem Cell Institute; Harvard NeuroDiscovery Center; Harvard Medical School Dean's Innovation Grant; Smith Family Foundation Odyssey Award; American Cancer Society (RSG-18-152-01-DDC), NIH (R01-AR070825 to Y.-C.H., 5R01 AR043369-23, 5R01CA222871, 5R01AR072304, 2P01 CA163222 to D.E.F., R01CA103846 and P01CA163222 to L.I.Z., DP2AT009499 and R01AI130019 to I.M.C.); grants from Dr. Miriam and Sheldon G. Adelson Medical Research Foundation to D.E.F.; Klarman Cell Observatory to A.R. Y.-C.H. is a Pew Scholar and a NYSCF – Robertson Investigator. A.R. and L.I.Z. are HHMI investigators; B.Z. is an awardee of the Charles A. King Trust Postdoctoral Research Fellowship; M.H. is an awardee of the NSF Graduate Research Fellowships Program (DGE1745303) and was supported by the Joint Program in Molecules, Cells, and Organisms (5T32GM007598-40); Y. Shwartz is a Helen Hay Whitney postdoctoral fellow and an awardee of the Woman in Science Weizmann Institute of Science Award; T.M.C. had a CAPES/HARVARD fellowship for visiting professor from CAPES (Process n. 88881.162285/2017-01) and is supported by a FAPESP grant (2013/08216-2). E.M.F. was supported by a Leukemia & Lymphoma Society Scholar grant (5372-15). J.D.B. and S.M. acknowledge support by the Broad Institute Fellows Program.

REFERENCES

1. Ephraim AJ On sudden or rapid whitening of the hair. *AMA Arch Derm* 79, 228–236 (1959). [PubMed: 13616721]
2. Navarini AA & Nobbe S Marie Antoinette syndrome. *Arch Dermatol* 145, 656–656 (2009). [PubMed: 19528420]
3. Alexander GM et al. Remote control of neuronal activity in transgenic mice expressing evolved G protein-coupled receptors. *Neuron* 63, 27–39 (2009). [PubMed: 19607790]
4. Zhu H et al. Cre-dependent DREADD (designer receptors exclusively activated by designer drugs) mice. *genesis* 54, 439–446 (2016). [PubMed: 27194399]
5. Müller-Röver S et al. A comprehensive guide for the accurate classification of murine hair follicles in distinct hair cycle stages. *Journal of Investigative Dermatology* 117, 3–15 (2001). [PubMed: 11442744]
6. Hsu Y-C, Li L & Fuchs E Emerging interactions between skin stem cells and their niches. *Nature Medicine* 20, 847–856 (2014).
7. Chang C-Y et al. NFIB is a governor of epithelial–melanocyte stem cell behaviour in a shared niche. *Nature* 495, 98–102 (2013). [PubMed: 23389444]
8. Rabbani P et al. Coordinated activation of Wnt in epithelial and melanocyte stem cells initiates pigmented hair regeneration. *Cell* 145, 941–955 (2011). [PubMed: 21663796]
9. Nishimura EK et al. Dominant role of the niche in melanocyte stem-cell fate determination. *Nature* 416, 854 (2002). [PubMed: 11976685]
10. Nishimura EK, Granter SR & Fisher DE Mechanisms of hair graying: incomplete melanocyte stem cell maintenance in the niche. *Science* 307, 720–724 (2005). [PubMed: 15618488]
11. Anthony TE et al. Control of stress-induced persistent anxiety by an extra-amygdala septohypothalamic circuit. *Cell* 156, 522–536 (2014). [PubMed: 24485458]
12. Ramirez S et al. Activating positive memory engrams suppresses depression-like behaviour. *Nature* 522, 335–339 (2015). [PubMed: 26085274]
13. Heidt T et al. Chronic variable stress activates hematopoietic stem cells. *Nat Med* 20, 754–758 (2014). [PubMed: 24952646]
14. Tye KM et al. Dopamine neurons modulate neural encoding and expression of depression-related behaviour. *Nature* 493, 537–541 (2013). [PubMed: 23235822]
15. Acs G, Biro T, Acs P, Modarres S & Blumberg PM Differential activation and desensitization of sensory neurons by resiniferatoxin. *J. Neurosci.* 17, 5622–5628 (1997). [PubMed: 9204943]
16. Baral P et al. Nociceptor sensory neurons suppress neutrophil and $\gamma\delta$ T cell responses in bacterial lung infections and lethal pneumonia. *Nature Medicine* 24, 417–426 (2018).

17. Ulrich-Lai YM & Herman JP Neural regulation of endocrine and autonomic stress responses. *Nature Reviews Neuroscience* 10, 397–409 (2009). [PubMed: 19469025]
18. Caterina MJ et al. The capsaicin receptor: a heat-activated ion channel in the pain pathway. *Nature* 389, 816–824 (1997). [PubMed: 9349813]
19. Kondo T & Hearing VJ Update on the regulation of mammalian melanocyte function and skin pigmentation. *Expert Rev Dermatol* 6, 97–108 (2011). [PubMed: 21572549]
20. Steingrímsson E, Copeland NG & Jenkins NA Melanocyte stem cell maintenance and hair graying. *Cell* 121, 9–12 (2005). [PubMed: 15820674]
21. Liao C-P, Booker RC, Morrison SJ & Le LQ Identification of hair shaft progenitors that create a niche for hair pigmentation. *Genes Dev.* 31, 744–756 (2017). [PubMed: 28465357]
22. Inomata K et al. Genotoxic stress abrogates renewal of melanocyte stem cells by triggering their differentiation. *Cell* 137, 1088–1099 (2009). [PubMed: 19524511]
23. Harris ML et al. A direct link between MITF, innate immunity, and hair graying. *PLOS Biology* 16, e2003648 (2018). [PubMed: 29723194]
24. Bosenberg M et al. Characterization of melanocyte-specific inducible Cre recombinase transgenic mice. *genesis* 44, 262–267 (2006). [PubMed: 16676322]
25. Köhler C et al. Mouse cutaneous melanoma induced by mutant BRAF arises from expansion and dedifferentiation of mature pigmented melanocytes. *Cell Stem Cell* 21, 679–693.e6 (2017). [PubMed: 29033351]
26. Moon H et al. Melanocyte stem cell activation and translocation initiate cutaneous melanoma in response to UV exposure. *Cell Stem Cell* 21, 665–678.e6 (2017). [PubMed: 29033353]
27. Sheng M & Greenberg ME The regulation and function of c-fos and other immediate early genes in the nervous system. *Neuron* 4, 477–485 (1990). [PubMed: 1969743]
28. Kostrzewa RM & Jacobowitz DM Pharmacological actions of 6-hydroxydopamine. *Pharmacol Rev* 26, 199–288 (1974). [PubMed: 4376244]
29. Boullin DJ, Costa E & Brodie BB Discharge of tritium-labeled guanethidine by sympathetic nerve stimulation as evidence that guanethidine is a false transmitter. *Life Sciences* 5, 803–808 (1966).
30. Acar M et al. Deep imaging of bone marrow shows non-dividing stem cells are mainly perisinusoidal. *Nature* 526, 126–130 (2015). [PubMed: 26416744]
31. Lay K, Kume T & Fuchs E FOXC1 maintains the hair follicle stem cell niche and governs stem cell quiescence to preserve long-term tissue-regenerating potential. *PNAS* 113, E1506–E1515 (2016). [PubMed: 26912458]
32. Wang L, Siegenthaler JA, Dowell RD & Yi R Foxc1 reinforces quiescence in self-renewing hair follicle stem cells. *Science* 351, 613–617 (2016). [PubMed: 26912704]
33. Cho IJ et al. Mechanisms, hallmarks, and implications of stem cell quiescence. *Stem Cell Reports* 12, 1190–1200 (2019). [PubMed: 31189093]
34. Nishimura EK et al. Key roles for transforming growth factor β in melanocyte stem cell maintenance. *Cell Stem Cell* 6, 130–140 (2010). [PubMed: 20144786]
35. Takeo M et al. EdnrB governs regenerative response of melanocyte stem cells by crosstalk with Wnt signaling. *Cell Reports* 15, 1291–1302 (2016). [PubMed: 27134165]
36. Tirosh I et al. Dissecting the multicellular ecosystem of metastatic melanoma by single-cell RNA-seq. *Science* 352, 189–196 (2016). [PubMed: 27124452]
37. Peters EMJ, Tobin DJ, Botchkareva N, Maurer M & Paus R Migration of melanoblasts into the developing murine hair follicle is accompanied by transient c-Kit expression. *J Histochem Cytochem.* 50, 751–766 (2002). [PubMed: 12019292]
38. Chou WC et al. Direct migration of follicular melanocyte stem cells to the epidermis after wounding or UVB irradiation is dependent on Mc1r signaling. *Nature Medicine* 19, 924–929 (2013).
39. Losiewicz MD, Carlson BA, Kaur G, Sausville EA & Worland PJ Potent inhibition of Cdc2 kinase activity by the flavonoid L86–8275. *Biochemical and Biophysical Research Communications* 201, 589–595 (1994). [PubMed: 8002990]
40. Wyatt PG et al. Identification of N-(4-Piperidinyl)-4-(2,6-dichlorobenzoylamino)-1H-pyrazole-3-carboxamide (AT7519), a novel cyclin dependent kinase inhibitor using fragment-based X-ray

- crystallography and structure based drug design. *J. Med. Chem* 51, 4986–4999 (2008). [PubMed: 18656911]
41. Borden P, Houtz J, Leach SD & Kuruville R Sympathetic innervation during development is necessary for pancreatic islet architecture and functional maturation. *Cell Rep* 4, 287–301 (2013). [PubMed: 23850289]
 42. Zeng X et al. Innervation of thermogenic adipose tissue via a calsyntenin 3 β -S100b axis. *Nature* 569, 229 (2019). [PubMed: 31043739]
 43. Katayama Y et al. Signals from the sympathetic nervous system regulate hematopoietic stem cell egress from bone marrow. *Cell* 124, 407–421 (2006). [PubMed: 16439213]
 44. Reed CM The ultrastructure and innervation of muscles controlling chromatophore expansion in the squid, *Loligo vulgaris*. *Cell Tissue Res.* 282, 503–512 (1995). [PubMed: 8581944]
 45. Fan SM-Y et al. External light activates hair follicle stem cells through eyes via an ipRGC–SCN–sympathetic neural pathway. *PNAS* 115, E6880–E6889 (2018). [PubMed: 29959210]
 46. Lerner AB Gray hair and sympathectomy. Report of a case. *Arch Dermatol* 93, 235–236 (1966). [PubMed: 5904034]
 47. Ortonne JP, Thivolet J & Guillet R Graying of hair with age and sympathectomy. *Arch Dermatol* 118, 876–877 (1982).
 48. Hinoi E et al. The sympathetic tone mediates leptin's inhibition of insulin secretion by modulating osteocalcin bioactivity. *J Cell Biol* 183, 1235–1242 (2008). [PubMed: 19103808]
 49. Abraira VE et al. The cellular and synaptic architecture of the mechanosensory dorsal horn. *Cell* 168, 295–310.e19 (2017). [PubMed: 28041852]
 50. Pruitt SC, Freeland A, Rusiniak ME, Kunnev D & Cady GK Cdkn1b overexpression in adult mice alters the balance between genome and tissue ageing. *Nat Commun* 4, 2626 (2013). [PubMed: 24149709]
 51. Szallasi A & Blumberg PM Resiniferatoxin, a phorbol-related diterpene, acts as an ultrapotent analog of capsaicin, the irritant constituent in red pepper. *Neuroscience* 30, 515–520 (1989). [PubMed: 2747924]
 52. Riol-Blanco L et al. Nociceptive sensory neurons drive interleukin-23-mediated psoriasiform skin inflammation. *Nature* 510, 157–161 (2014). [PubMed: 24759321]
 53. Kashem SW et al. Nociceptive sensory fibers drive interleukin-23 production from CD301b+ dermal dendritic cells and drive protective cutaneous immunity. *Immunity* 43, 515–526 (2015). [PubMed: 26377898]
 54. Marshall ICB et al. Activation of vanilloid receptor 1 by resiniferatoxin mobilizes calcium from inositol 1,4,5-trisphosphate-sensitive stores. *British Journal of Pharmacology* 138, 172–176 (2003). [PubMed: 12522087]
 55. Neubert J et al. Peripherally induced resiniferatoxin analgesia. *Pain* 104, 219–228 (2003). [PubMed: 12855332]
 56. Watanabe T, Sakurada N & Kobata K Capsaicin-, resiniferatoxin-, and olvanil-induced adrenaline secretions in rats via the vanilloid receptor. *Bioscience, Biotechnology, and Biochemistry* 65, 2443–2447 (2001).
 57. Zhang Bing, He M & Hsu Y-C FACS isolation of melanocyte stem cells from mouse skin. *Protoc. Exch* (2019). DOI: 10.21203/rs.2.17987/v1.
 58. Gilchrist BA, Vrabel MA, Flynn E & Szabo G Selective cultivation of human melanocytes from newborn and adult epidermis. *J. Invest. Dermatol* 83, 370–376 (1984). [PubMed: 6491362]
 59. Dobin A et al. STAR: ultrafast universal RNA-seq aligner. *Bioinformatics* 29, 15–21 (2013). [PubMed: 23104886]
 60. Love MI, Huber W & Anders S Moderated estimation of fold change and dispersion for RNA-seq data with DESeq2. *Genome Biology* 15, 550 (2014). [PubMed: 25516281]
 61. Huang DW, Sherman BT & Lempicki RA Bioinformatics enrichment tools: paths toward the comprehensive functional analysis of large gene lists. *Nucleic Acids Res.* 37, 1–13 (2009). [PubMed: 19033363]
 62. Huang DW, Sherman BT & Lempicki RA Systematic and integrative analysis of large gene lists using DAVID bioinformatics resources. *Nat Protoc* 4, 44–57 (2009). [PubMed: 19131956]

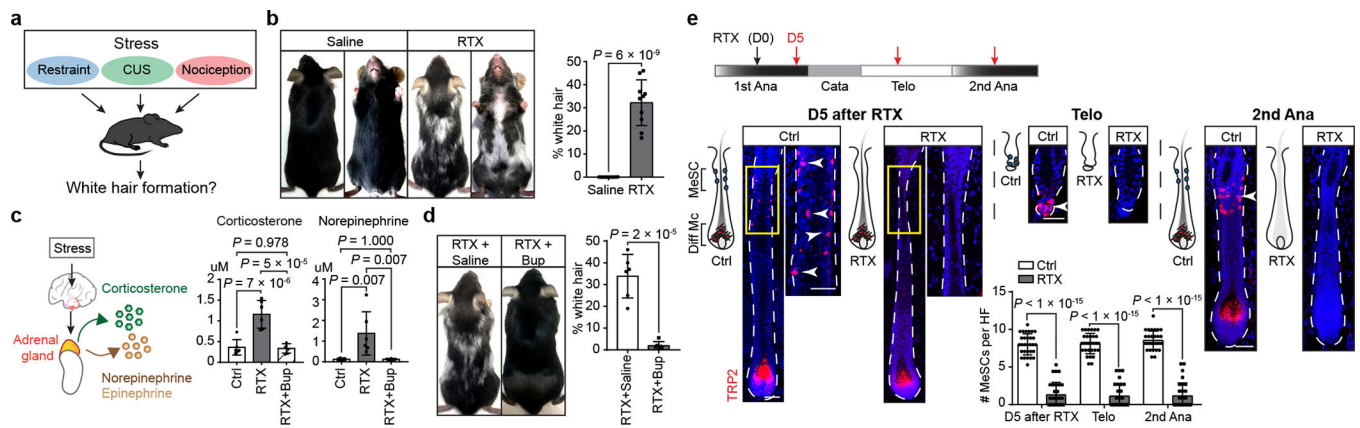


Fig. 1 | Stress depletes melanocyte stem cells (MeSCs).

a, Black coat C57BL/6J mice are subjected to different stress models. **b**, Hair greying after resineratoxin (RTX) injection. Right, quantification of skin area covered by white hairs ($n = 10$ mice for each condition, two-tailed unpaired t -test). **c**, Liquid chromatography with tandem mass spectrometry (LC-MS-MS) quantifies serum stress hormone concentrations after injection of RTX alone or in combination with buprenorphine (Bup, $n = 6$ mice for each condition, one-way ANOVA with Tukey's multiple comparisons). **d**, Injection of RTX with buprenorphine blocks white hair formation ($n = 6$ mice for each condition, two-tailed unpaired t -test). **e**, Upper panel, experimental design (black arrow: RTX injection, red arrows: harvesting). Lower panels, immunofluorescent staining for TRP2 (melanocyte lineage marker) in the hair follicle (HF) of control (Ctrl, saline-injected) and RTX injected mice ($n = 30$ HF's throughout the skin from 6 mice for each condition, two-way ANOVA with original FDR method of Benjamini and Hochberg). Yellow boxes denote the upper HF region where MeSCs reside. Enlarged views are shown to the right. Arrowheads: MeSCs. CUS: chronic unpredictable stress. D: day. Ana: anagen. Cata: catagen. Telo: telogen. Diff Mc: differentiated melanocytes. Scale bars, 50 μ m. All data are mean \pm S.D.

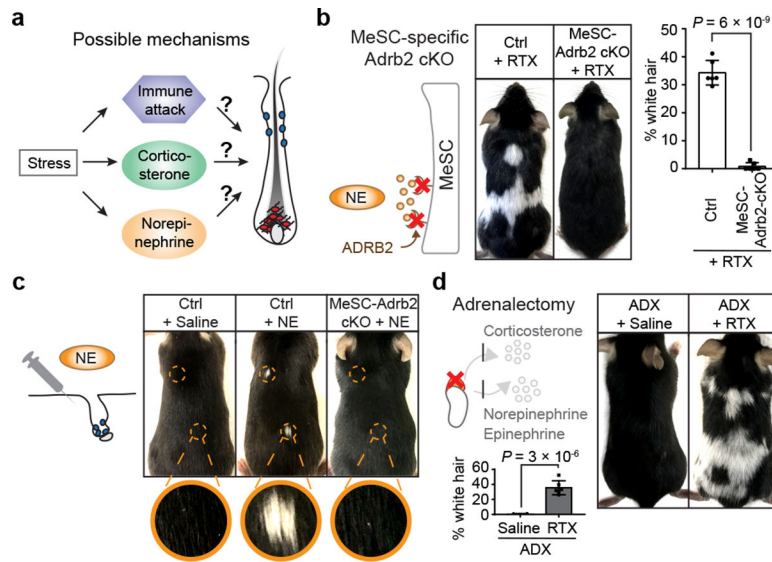


Fig. 2 |. Norepinephrine drives hair greying.

a, Possible mechanisms of MeSC loss. **b**, RTX injection into Tyr-CreER; *Adrb2* fl/fl (MeSC-Adrb2 cKO) mice fails to trigger hair greying ($n = 6$ mice for each condition, two-tailed unpaired t -test). **c**, White hair formation in norepinephrine injection sites (NE; $n = 10$ injected sites from 8 mice for each condition. Quantifications see Extended data Fig. 4e). Yellow dashed circles denote intradermal injection sites. **d**, White hair formation after RTX injection in adrenalectomized mice (ADX, $n = 6$ mice for each condition, two-tailed unpaired t -test). All data are mean \pm S.D.

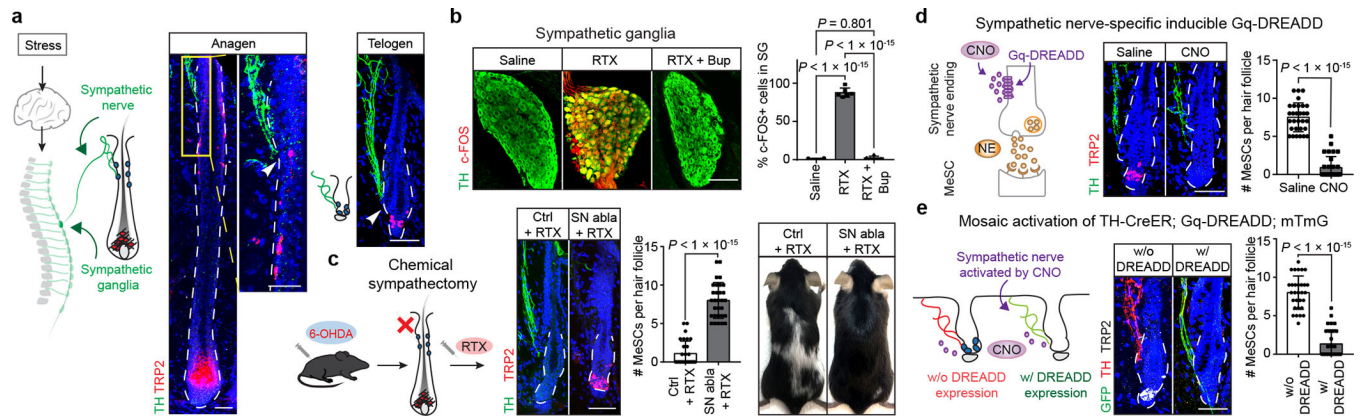


Fig. 3 |. Hyperactivation of the sympathetic nervous system depletes MeSCs.

a, Sympathetic nerve innervates MeSC niches. White arrowhead indicates the close proximity of nerve endings to MeSCs ($n = 6$ mice for each condition). **b**, Immunofluorescent staining of sympathetic ganglia for tyrosine hydroxylase (TH, green) and c-FOS (red) from mice injected with saline, RTX, and RTX with buprenorphine ($n = 6$ ganglia from 3 mice for each condition, one-way ANOVA with Tukey's multiple comparisons). **c**, 6-hydroxydopamine (6-OHDA) injection blocks MeSC loss and white hair induction by RTX ($n = 30$ HF from 6 mice for each condition, two-tailed unpaired t -test. See also Extended data Fig. 5d). **d**, Left, schematic of sympathetic nerve activation using a Gq-DREADD system. Right, immunofluorescent staining for TH (green) and TRP2 (red) from TH-CreER; Gq-DREADD mice treated with saline or Clozapine N-Oxide (CNO, $n = 30$ HF from 6 mice for each condition, two-tailed unpaired t -test). **e**, Mosaic activation of sympathetic nerves using TH-CreER; Gq-DREADD; Rosa-mT/mG mice. Bar graphs quantify the number of MeSCs in HF innervated by DREADD negative sympathetic nerves (w/o DREADD) vs. DREADD positive sympathetic nerves (w/ DREADD, marked by membrane GFP expression). $n = 30$ HF for each condition from 4 mice, two-tailed unpaired t -test. SN abla: sympathetic nerve ablation. Scale bars, 50 μ m. All data are mean \pm S.D.

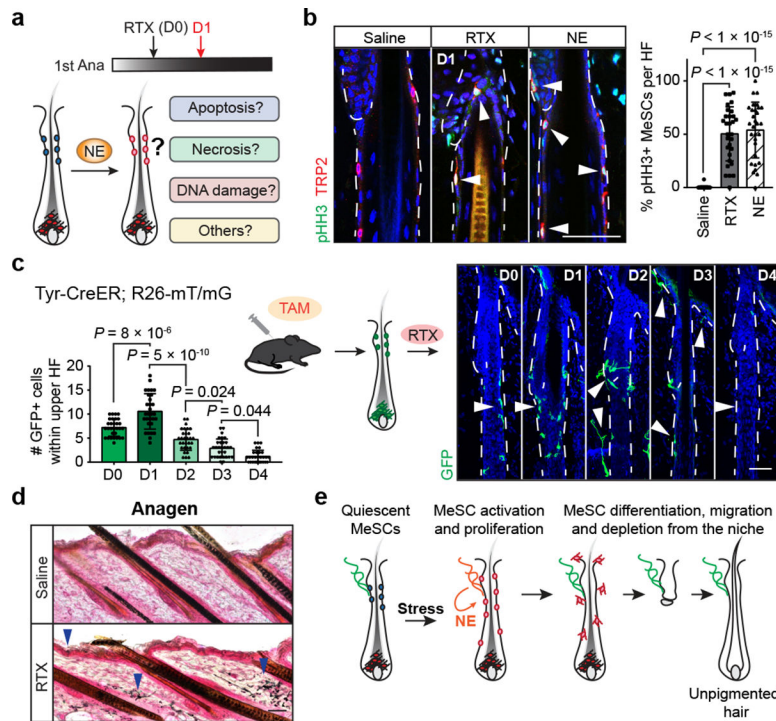


Fig. 4 |. Norepinephrine drives MeSCs out of quiescence.

a, Possible mechanisms by which norepinephrine depletes MeSCs. **b**, Immunofluorescent staining for Phospho-Histone H3 (pHH3, green) and TRP2 (red) 1 day after RTX or norepinephrine injection. White arrowhead highlights the proliferative MeSCs ($n = 30$ HF) from 5 mice for each condition, one-way ANOVA with Tukey's multiple comparisons). **c**, Time-course of MeSC behaviour after RTX treatment in Tyr-CreER; R26-mT/mG mice. White arrowheads mark MeSCs ($n = 30$ HF) from 3 mice for each timepoint, one-way ANOVA with Tukey's multiple comparisons). **d**, Fontana–Masson melanin staining 5 days after saline or RTX injection ($n = 6$ mice for each condition). Blue arrowheads indicate ectopic pigments. **e**, Model summarizing steps of stress-induced MeSC depletion. TAM: tamoxifen. Scale bars, $50 \mu\text{m}$. All data are mean \pm S.D.

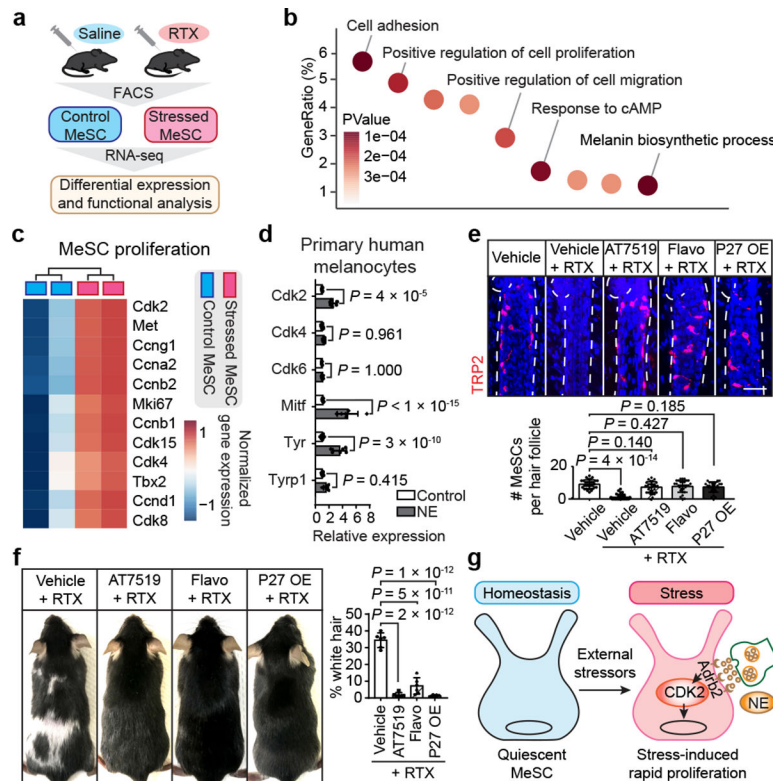


Fig. 5 |. Inhibition of aberrant MeSC proliferation prevents stress-induced hair greying.
a, Experimental workflow. FACS at telogen. **b**, Gene ontology enrichment analysis of significantly dysregulated genes in stressed MeSCs ($n = 2$ biologically independent samples for each condition, Fisher exact test). **c**, Heatmaps of signature gene expression related to MeSC proliferation ($n = 2$ biologically independent samples for each condition). **d**, qRT-PCR of MeSC proliferation and differentiation genes in cultured primary human melanocytes treated with norepinephrine ($n = 6$ samples from three independent donors, two-way ANOVA with original FDR method of Benjamini and Hochberg). **e**, Immunofluorescent staining for TRP2 (red) from mice 5 days after treatments of RTX together with AT7519, Flavopiridol, or with MeSC-specific P27 overexpression (P27 OE, $n = 30$ HF from 6 mice each condition, one-way ANOVA with Tukey's multiple comparisons). **f**, Topical treatment of AT7519, Flavopiridol, or MeSC-specific P27 overexpression inhibits RTX-induced hair greying ($n = 6$ mice for each condition, one-way ANOVA with Tukey's multiple comparisons). **g**, Model summarizing the main findings. Under strong external stressors, activated sympathetic nerves secrete norepinephrine that binds to ADRB2 on MeSCs. NE-ADRB2 signalling drives rapid MeSC proliferation, followed by ectopic differentiation and exhaustion. Flavo: Flavopiridol. Scale bars, 50 μm . All data are mean \pm S.D.